INTERNATIONAL JOURNAL OF CLIMATOLOGY
Int. J. Climatol. (2016)
Published online in Wiley Online Library
(wileyonlinelibrary.com) DOI: 10.1002/joc.4881

RMetS
Royal Meteorological Society

Association between three prominent climatic teleconnections and precipitation in Iran using wavelet coherence

Alireza Araghi,[a]* Mohammad Mousavi-Baygi,[a] Jan Adamowski[b] and Christopher Martinez[c]

[a] *Department of Water Engineering, Faculty of Agriculture, Ferdowsi University of Mashhad, Iran*

[b] *Department of Bioresource Engineering, Faculty of Agriculture and Environmental Sciences, McGill University, Sainte-Anne-de-Bellevue, Canada*

[c] *Department of Agricultural and Biological Engineering, Institute of Food and Agricultural Sciences, University of Florida, Gainesville, FL, USA*

ABSTRACT: Large-scale climatic teleconnections have noticeable effects on meteorological events in different regions of the world. In this study, the linkages between three major climatic indices, Arctic Oscillation (AO), North Atlantic Oscillation (NAO) and Southern Oscillation Index (SOI), and precipitation in Iran were assessed from 1960 to 2014, at 30 synoptic stations in a time-frequency space, using wavelet coherence (WCO). The results showed that the SOI is the most effective climatic teleconnection on precipitation in Iran, although the other studied climatic indices have noticeable effects as well. The predominant and effective period of AO on precipitation was equal to or greater than 32 months at most of the stations, while the major effective period of NAO was equal to or greater than 64 months. For the SOI, most parts of the country were affected by a period of less than 64 months, while the predominant period of SOI for the northwestern part of the country was greater than 64 months. A uniform phase difference was not observed between the three studied climatic indices and precipitation in the country; instead the phase differences were usually random. For long-term periods of SOI, an anti-phase situation was detected at most of the stations. The study suggested that the WCO is a very powerful and flexible method for studying the relationship between multiple time series in a time–frequency space, and its application in hydrological and meteorological research is expected to increase in the near future.

KEY WORDS Arctic Oscillation; North Atlantic Oscillation; Southern Oscillation Index; Precipitation; Wavelet coherence; Iran

Received 12 November 2015; Revised 8 August 2016; Accepted 9 August 2016

1. Introduction

Precipitation has a major influence on hydrological elements, water resources, agricultural productivity, urban infrastructural activities and many other aspects of life and the environment (Mavi and Tupper, 2004; Loucks and van Beek, 2005; Wilhite, 2005; Karamouz *et al.*, 2013; Ahrens, 2016). It is well known that precipitation is a complex phenomenon that is affected by different microscale and macroscale atmospheric and geographic factors (Curry and Webster, 1999; Li and Gao, 2012). Topography, land use, distance to large water resources and dominant atmospheric systems are some of the factors that affect the amount and intensity of precipitation in a region (McCuen, 1998; Rakhecha and Singh, 2009; Shelton, 2009). Large-scale atmospheric activities, known as climatic teleconnections, can have noticeable effects on the climate of a wide range of locations on Earth (Curry and Webster, 1999; Bosart and Bluestein, 2008). Thermal interactions and humidity exchanges that occur between oceans surfaces and the atmosphere constitute substantial fuel for creating large-scale atmospheric phenomena (Saha, 2008; Mak, 2011; Lutgens and Tarbuck, 2013). Furthermore, it is well known that meteorological, hydrological and even agricultural components are strongly influenced by large-scale atmospheric and oceanic fluctuations (Gan *et al.*, 2007; Martinez *et al.*, 2009; Karamouz *et al.*, 2013). Therefore, finding the association between meteorological elements and the oscillatory pattern of climatic teleconnections can be very helpful in improving the accuracy of hydro-meteorological predictions. In recent years, researchers have tried to employ various methodologies to find the relationship between precipitation parameters and climatic teleconnections [e.g. Arctic Oscillation (AO), North Atlantic Oscillation (NAO), El Niño-Southern Oscillation (ENSO), Pacific Decadal Oscillation (PDO), Southern Oscillation Index (SOI), etc.] in different regions of the world (Yarnal and Diaz, 1986; Shabbar *et al.*, 1997; Cayan *et al.*, 1998; Coulibaly, 2006; Jiang *et al.*, 2014).

Signal analysis and remote sensing analysis have been used to reveal relationships between precipitation and climatic teleconnections (Chang *et al.*, 2014; Niu *et al.*, 2014; Di *et al.*, 2015). In contrast to many atmospheric variables (e.g. temperature, vapour pressure, relative humidity, etc.), precipitation shows a very complex and non-uniform fluctuation pattern over time (Von Storch and Zwiers, 1999; Duhan and Pandey, 2013). Accordingly,

* Correspondence to: A. Araghi, Department of Water Engineering, Faculty of Agriculture, Ferdowsi University of Mashhad, Khorasan Razavi, Mashhad 9177948974, Iran. E-mail: araghi.a@stu.um.ac.ir; alireza_araghi@yahoo.com

the methods employed for precipitation analysis should have adequate power to accurately extract and detect the periodic attributes of the precipitation time series. Wavelet transform (WT) is one of the most powerful and applicable mathematical methods in signal processing and time series analysis and it is now commonly used in meteorology and hydrology studies (Labat, 2005; Labat *et al.*, 2005; Adamowski *et al.*, 2009; Adamowski and Chan, 2011; Sang, 2013; Nourani *et al.*, 2014). WT is a useful method to find the associations between two signals or time series, especially when these time series are non-stationary and uniform seasonality patterns do not exist in the time series (e.g. precipitation and streamflow) (Hernández and Weiss, 1996; Adamowski and Prokoph, 2013; Adamowski *et al.*, 2013).

Previous studies have shown WT to be a trustworthy method to identify the relationship between hydro-meteorological or environmental elements and climatic teleconnections. For instance, wavelet-based analysis was applied to the analysis of the association of seasonal precipitation and hydrologic variability with climatic teleconnections for regions of Alberta and southwestern Canada (Gan *et al.*, 2007; Mwale *et al.*, 2009; Jiang *et al.*, 2014). In another study WTs served to investigate the relationship between the variation in lake water levels and the NAO index for seven lakes scattered across Turkey (Küçük *et al.*, 2009). The study showed that NAO had a significant influence on these lakes' water levels. Using WTs Kuo *et al.* (2010) assessed the variability of seasonal rainfall in Taiwan (1974–2006) and its linkage to large scale climatic oscillations. Predominantly employing WTs Rossi *et al.* (2011) analyzed time-scale variability of well-known climatic teleconnections (1900–2009). In another study in Turkey, temporal and spatial patterns in precipitation variability, gleaned from 1961–2008 data from 271 climatological stations, and its association with climatic teleconnections were probed using continuous WT techniques (Unal *et al.*, 2012). The potential impacts of ENSO, NAO and PDO on precipitation regimes were assessed in the upper Medjerda basin, northern Tunisia, using cross-wavelet analysis (Ouachani *et al.*, 2013). In another study, multiple large-scale climatic indices were used as predictors for streamflow forecasting in west-central Florida (Risko and Martinez, 2014). Drawing on data from 46 hydrological stations in Romania (1935–2010), wavelet analysis was used to study the spatial and temporal variability of winter streamflow and its linkage with AO, NAO along with some other large-scale climate patterns (Ionita *et al.*, 2014). Chang *et al.* (2014) studied the relationship between regional precipitation regimes in Panama and Central America, and NAO and ENSO using an integrated method based on wavelet analysis and remote sensing techniques. The spatial and temporal variability of drought and its association with large-scale climate indices in an arid region of China was studied using wavelet analysis (Wang *et al.*, 2015).

Though studies focusing on the detection of linkages between hydro-meteorological elements and climatic teleconnections via WTs have increased in recent years, there remains a need to broaden the scope of studies investigating hydrology and climatic teleconnection interactions within a time–frequency space to a wider range of regions across the world. In the present paper, the previously unexplored associations between three major large-scale climatic teleconnections (AO, NAO and SOI) and monthly precipitation at 30 synoptic stations in Iran (1960–2014) were studied. The present investigators were particularly interested in analysing the influences of certain major but spatially distant global teleconnections on precipitation in Iran. Accordingly, regional climatic indices (e.g. Indian Ocean Dipole) were ignored.

A theoretical background of WTs and wavelet coherence (WCO) is provided in Section 2, followed by a description and discussion of the precipitation data and large-scale climatic indices used in this research in Section 3. The methodology employed in this study is explained in Section 4, and finally the results and discussions are presented in Section 5.

2. Theoretical background

2.1. Wavelet transform

Various methods have been introduced for signal processing and time series analysis. Most of these methods are mathematical transforms that convert vectors or functions from one space to another. The major benefit provided by mathematical transformations is feature extraction, which aids in simplifying the detection of signals and time series features (Kreyszig, 2011). Some of the transformations [e.g. Fourier transforms (FTs)] are only appropriate for the analysis of stationary time series exhibiting a uniform oscillation pattern over time (Oppenheim *et al.*, 1999). These transformations are not robust enough for the analysis of non-stationary time series, since they cannot identify all frequencies within the time series (Percival and Walden, 2000). WT is a powerful and accurate mathematical transformation, widely used for signal processing (Hernández and Weiss, 1996; Nievergelt, 2001; Olkkonen, 2011) and time series analysis (Percival and Walden, 2000; Sang, 2013). The theory behind WT is relatively similar to that of FTs, but offers much greater flexibility (Fugal, 2009), allowing a highly accurate capture of all frequencies (e.g. stationary/nonstationary, short term/long term, etc.) present in a given time series (Percival and Walden, 2000). The WT of a time series $x(t)$, is defined as (Grossmann and Morlet, 1984; Liu, 1994; Partal and Küçük, 2006; Adamowski *et al.*, 2009):

$$W(s.\tau) = \frac{1}{\sqrt{s}} \int_{-\infty}^{+\infty} x(t)\ \psi^* \left(\frac{t-\tau}{s} \right) dt \qquad (1)$$

$$\psi_{(s.\tau)}(t) = \frac{1}{\sqrt{s}} \psi \left(\frac{t-\tau}{s} \right) \qquad (2)$$

where $W(s.\tau)$ is a WT with a scale of s and a time shift of τ. While ψ represents the wavelet function, ψ^* denotes the complex conjugate. If $\tau = 0$ and $s = 1$ then $\psi(t)$ represents the basic or 'mother' wavelet (Mallat, 2008). Variations

Table 1. General identification and some of the basic statistics of annual precipitation (1960–2014) in the selected synoptic stations.

No.	Station name	Longitude (°E)	Latitude (°N)	Elevation (m)	Climate	Mean (mm)	Standard deviation (mm)	Minimum (mm)	Maximum (mm)
1	Abadan	48.25	30.37	6.6	Arid	150.3	60.3	36.8	297.9
2	Ahwaz	48.67	31.33	22.5	Arid	220.8	83.5	72.9	468.8
3	Arak	49.77	34.1	1708	Semi-arid	330.1	96.6	128.1	606.6
4	Babolsar	52.65	36.72	−21	Humid	897.3	171.2	486.2	1325.6
5	Bam	58.35	29.1	1066.9	Arid	58.3	27.4	14.6	131.2
6	Bandar Abbas	56.37	27.22	98	Arid	168.6	111.4	1	494.7
7	Birjand	59.2	32.87	1491	Arid	162.2	50.2	64.6	292.7
8	Bushehr	50.83	28.98	196	Arid	238.9	111	19.4	671.3
9	Esfahan	51.67	32.62	1550.4	Arid	122.2	48.9	40.2	250
10	Ghazvin	50.05	36.25	1279.2	Semi-arid	314.8	86.3	155.6	515.7
11	Gorgan	54.27	36.85	133	Sub-humid	574.5	117.3	314.6	847.3
12	Hamedan	48.72	35.2	1679.7	Semi-arid	313.5	92.1	12.6	517.7
13	Kerman	56.97	30.25	1753	Arid	138.4	46.4	41.2	263.6
14	Kermanshah	47.15	34.35	1318.6	Semi-arid	436.9	124.6	147.3	784.5
15	Khorramabad	48.28	33.43	1147.8	Semi-arid	489.5	121.3	237.1	771.1
16	Khoy	44.97	38.55	1103	Semi-arid	289.7	78.9	148.1	526.1
17	Mashhad	59.63	36.27	999.2	Semi-arid	248.8	71.5	121.4	427.1
18	Ramsar	50.67	36.9	−20	Humid	1215.8	289.8	755.4	1934.2
19	Rasht	49.6	37.25	−6.9	Humid	1329.7	255.3	831.3	1967.6
20	Sabzevar	57.72	36.2	977.6	Arid	187.3	60.3	58	311.4
21	Sanandaj	47	35.33	1373.4	Semi-arid	439.6	118.5	200.3	779.5
22	Shahrekord	50.85	32.28	2048.9	Semi-arid	326.8	91.3	140.9	527.5
23	Shahroud	54.95	36.42	1345.3	Arid	155.1	55.4	63.2	343.3
24	Shiraz	52.6	29.53	1484	Semi-arid	313.6	107	96.3	621.9
25	Tabriz	46.28	38.08	1361	Arid	281.6	81	148	547.5
26	Tehran	51.32	35.68	1190.8	Semi-arid	231.9	72.7	100.3	399.4
27	Torbat Heydarieh	59.22	35.27	1450.8	Semi-arid	259.5	82	82.1	416.5
28	Yazd	54.28	31.9	1237.2	Arid	55.9	25.9	9.3	118.4
29	Zahedan	60.88	29.47	1370	Arid	80.9	39.1	18.3	173.1
30	Zanjan	48.48	36.68	1663	Semi-arid	305.1	77.9	142.5	481.1

in s provide the WT its flexibility, and therefore its ability to capture all short or long frequency events in a time series. At each time shift, τ, and each scale, s, the similarity of $x(t)$ and ψ is calculated on the basis of inner product theory, in a manner roughly equivalent to a FT (Equations 1 and 2). Like other correlation methods, larger values of $W(s.\tau)$ indicate a stronger relationship between $x(t)$ and ψ for specific values of s and τ (Adamowski and Sun, 2010). In general, any time series can be decomposed to its fundamental high and low frequencies via WT. When $s>1$, ψ corresponds to a high frequency (Mallat, 2008).

Generally, there are two types of WT, continuous WT (CWT) and discrete WT (DWT). The CWT generates longer series of $W(s.\tau)$ since the scale factor is not limited, while in DWT the scale factor is usually dyadic (Olkkonen, 2011; Araghi *et al.*, 2015). The dyadic scale means that the scales in a DWT are based on powers of 2, in the form of 2^j, where j corresponds to the frequency range. In other words, in the CWT the value of s follows an arithmetic progression, whereas in the DWT it follows a geometric progression. Thus, although DWT shows adequate precision for time-frequency analysis and has a faster calculation process, some scales will be ignored. Previous studies have shown that the DWT produces more accurate results for the analysis of stationary time series with uniform fluctuations over time, such as air temperature, compared to non-stationary series without seasonality patterns (Nalley *et al.*, 2013; Araghi *et al.*, 2015).

Generally, the phase indicates the specific point in a waveform cycle, usually measured as an angle in degrees. Using phase enables one to explore the relative displacement between or among two signals, which is normally called the phase difference. Leading (lagging) phase refers to a signal that occurs ahead (behind) of another signal. When two signals have no phase differences, they are called in-phase, and when they have a difference equal to 180°, they are called anti-phase. When information about phase interactions between two time series is required, continuous complex wavelet functions are a better choice (Mallat, 2008). The wavelet function (ψ) is generally a function with a zero mean that is localized in time and frequency. Until now, various wavelet functions have been presented; some of these functions have real outputs and others have complex outputs (Lau and Weng, 1995). The Morlet wavelet is one of the most popular complex wavelet functions that is widely used in geophysical and hydro-climatological studies, and it is defined in Equation (3) (Grinsted *et al.*, 2004; Maraun and Kurths, 2004).

$$\varphi_0(\theta) = \pi^{-1/4} e^{j\omega_0\theta} e^{-\theta^2/2} \tag{3}$$

where φ_0 is the Morlet wavelet function, ω_0 and θ are dimensionless frequency and time, respectively. The

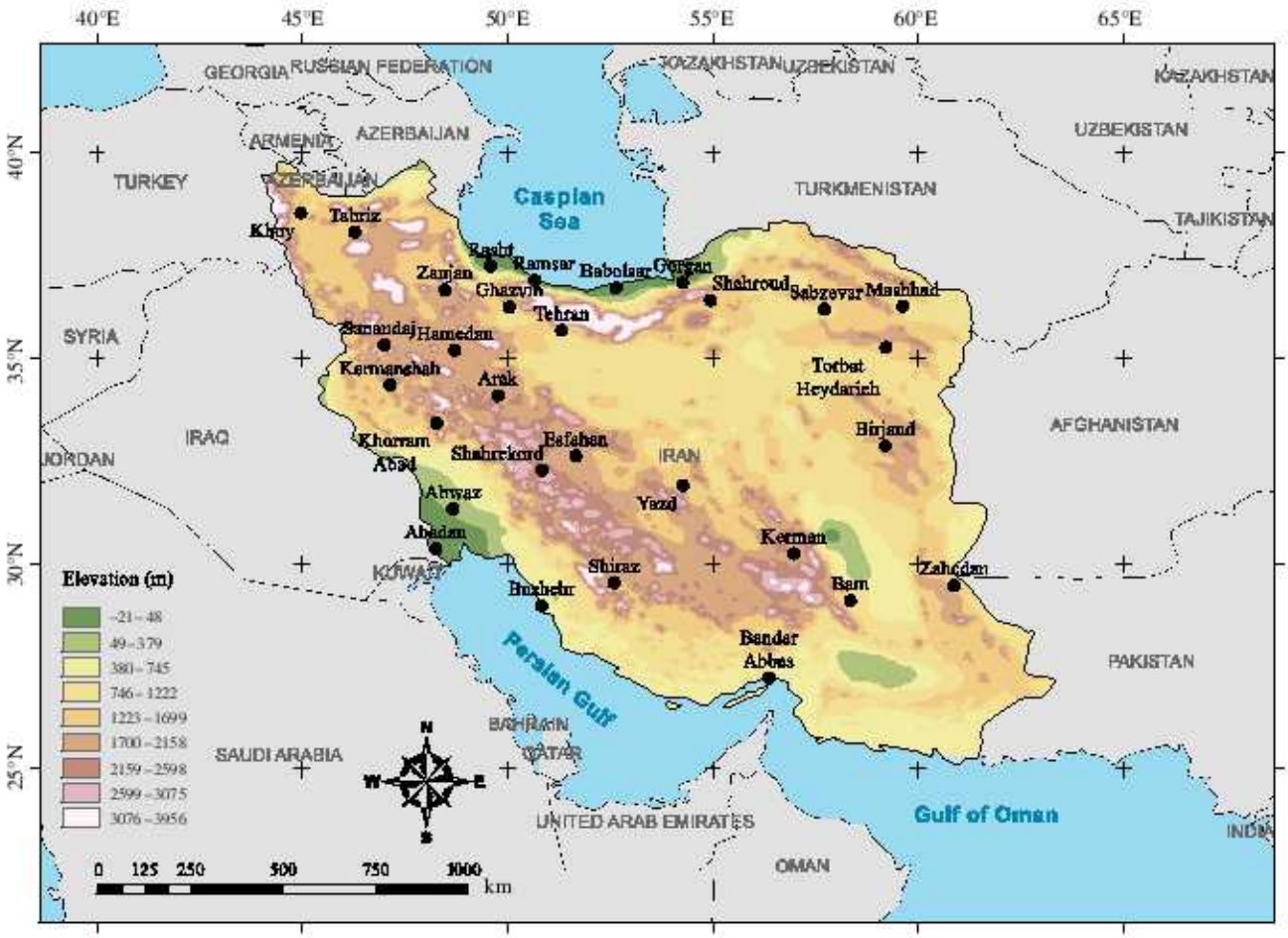

Figure 1. The location of the selected synoptic stations (filled black circles) in Iran used for this study.

wavelet location in time can be specified by $e^{-\theta^2/2}$ (Gaussian envelope). When ω_0 is high (low), the resolution of scale will increase (decrease) and the resolution of time will decrease (increase). The time and scale resolutions can be adjusted by ω_0. It should be noted that the resolution in time and scale belongs to the size of the window function, and the lower (higher) resolution will be a better choice when the fluctuations in the time series mostly occur in the long (short) term. The Morlet wavelet is well localized in scale, and accordingly, a high resolution in frequency is achieved using this wavelet function (Mallat, 2008). In addition, the complex WT obtained from applying the Morlet wavelet (Equation (3)) to the time series allows for the separation of the phase and the amplitude in any time series (Torrence and Compo, 1998; Grinsted *et al.*, 2004). As previously discussed, the wavelet function moves across the length of a time series from beginning to end. Hence, the edge parts in the beginning and end sections of a time series have noticeable effects on the wavelet coefficients, which are usually called the edge effects. The area in which the edge discontinuity affects the wavelet power (i.e. squared absolute-value of the wavelet coefficients, $|W|^2$, based on the Equation (1)) is called the cone of influence (COI), which drops to e^{-2} of the values at the edge of the time series (Torrence and Compo, 1998). Therefore, interpreting the wavelet power based on the significant regions inside or mostly across the COI area is not a reasonable approach. The COI is specified by a shadow overlay and with dotted lines in all of the figures in this paper.

2.2. Wavelet coherence

In a time series analysis, the autocorrelation function (ACF) represents the major lags of time at which the time series is correlated with itself (Box *et al.*, 2008). The wavelet power spectrum (WPS) can be defined similarly to the ACF, but in time–frequency (or time-scale) space (Torrence and Compo, 1998; Maraun and Kurths, 2004). The WPS shows the power spectrum of the time series $x(t)$ at a certain time, t_i, and for a specific scale, s. The WPS is defined as follows (Grinsted *et al.*, 2004; Maraun and Kurths, 2004):

$$\mathrm{WPS}_{t_i}(s) = \left\langle W_{t_i}(s)\ W_{t_i}(s)^* \right\rangle \qquad (4)$$

where the $\langle \ldots \rangle$ indicate the expectation values, and $W_{t_i}(s)^*$ is the complex conjugate of $W_{t_i}(s)$. As can be seen in Equation (4), both of the WTs belong to the time series $x(t)$, hence the notation of x is ignored in all of the items in this equation. However, in many cases, for example in climatological or hydrological analysis, one is interested in

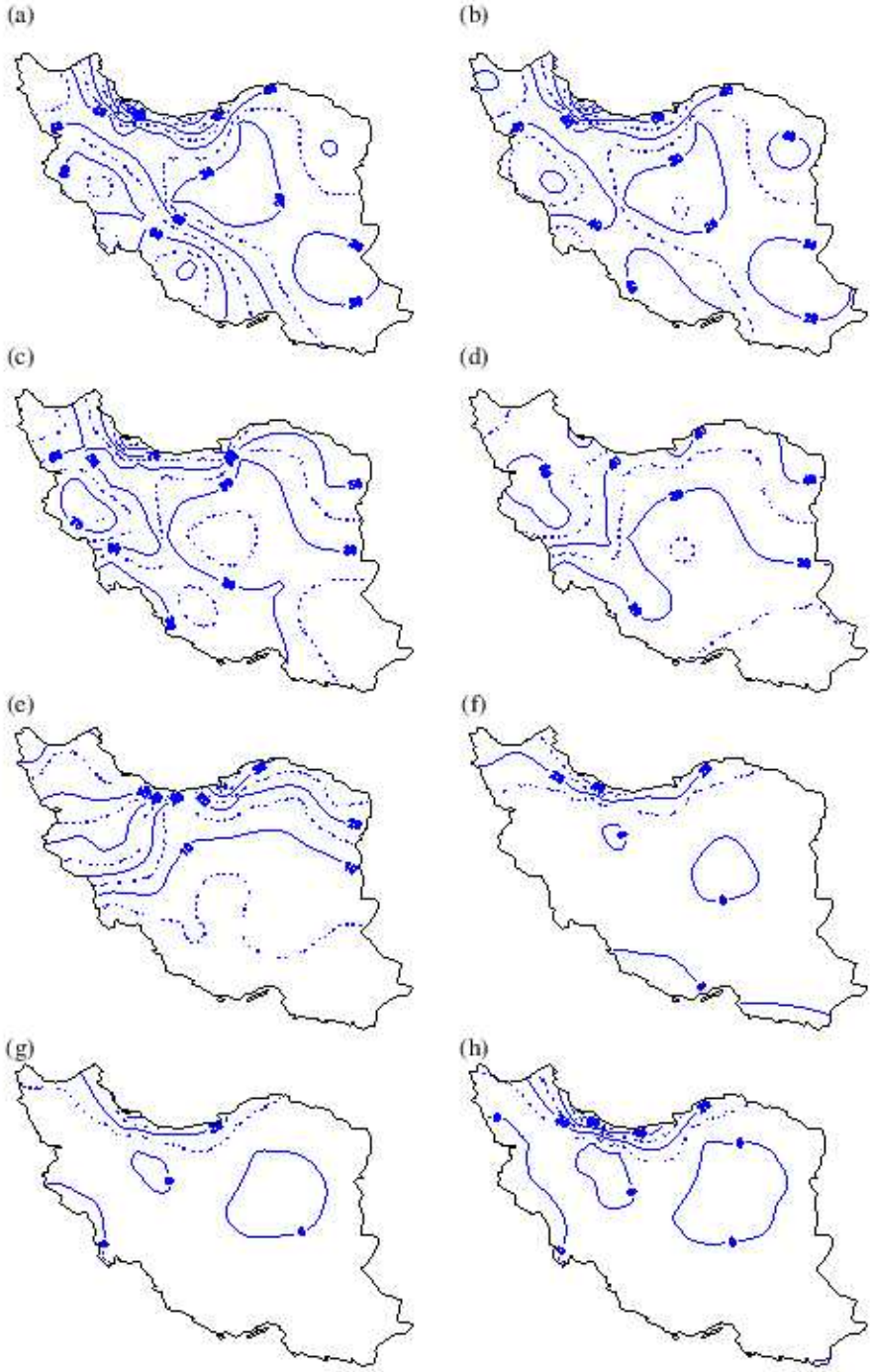

Figure 2. Average precipitation (mm) during 1960–2014 in Iran from January to August (a–h).

finding the correlation between two signals or time series in a time–frequency space. The WPS turns into the wavelet cross spectrum (WCS) when the correlation between two time series is interested to achieve. The equation of WCS is similar to the WPS, but it is written for $x(t)$ and $y(t)$ WTs (Torrence and Compo, 1998; Grinsted *et al.*, 2004).

$$\mathrm{WCS}_{I_i}(s) = \left\langle W^x_{I_i}(s)\ W^y_{I_i}(s)^* \right\rangle \tag{5}$$

where $W^x_{I_i}(s)$ and $W^y_{I_i}(s)^*$ are the WT and the complex conjugate of the WT for the time series $x(t_i)$ and $y(t_i)$, respectively. The complex conjugate of the WT is needed for the second time series, similar to the WPS (Torrence and Compo, 1998). In contrast to the WPS, values of the WCS are complex, and hence, can be decomposed into amplitude and phase as follows (Torrence and Webster, 1999; Grinsted *et al.*, 2004; Cazelles *et al.*, 2008):

$$\mathrm{WCS}_{I_i}(s) = \left|\mathrm{WCS}_{I_i}(s)\right| e^{I\phi_I(s)} \tag{6}$$

$$\phi_i(s) = tan^{-1}\frac{\Im\left(\left\langle W^x_{I_i}(s)\ W^y_{I_i}(s)^*\right\rangle\right)}{\Re\left(\left\langle W^x_{I_i}(s)\ W^y_{I_i}(s)^*\right\rangle\right)} \tag{7}$$

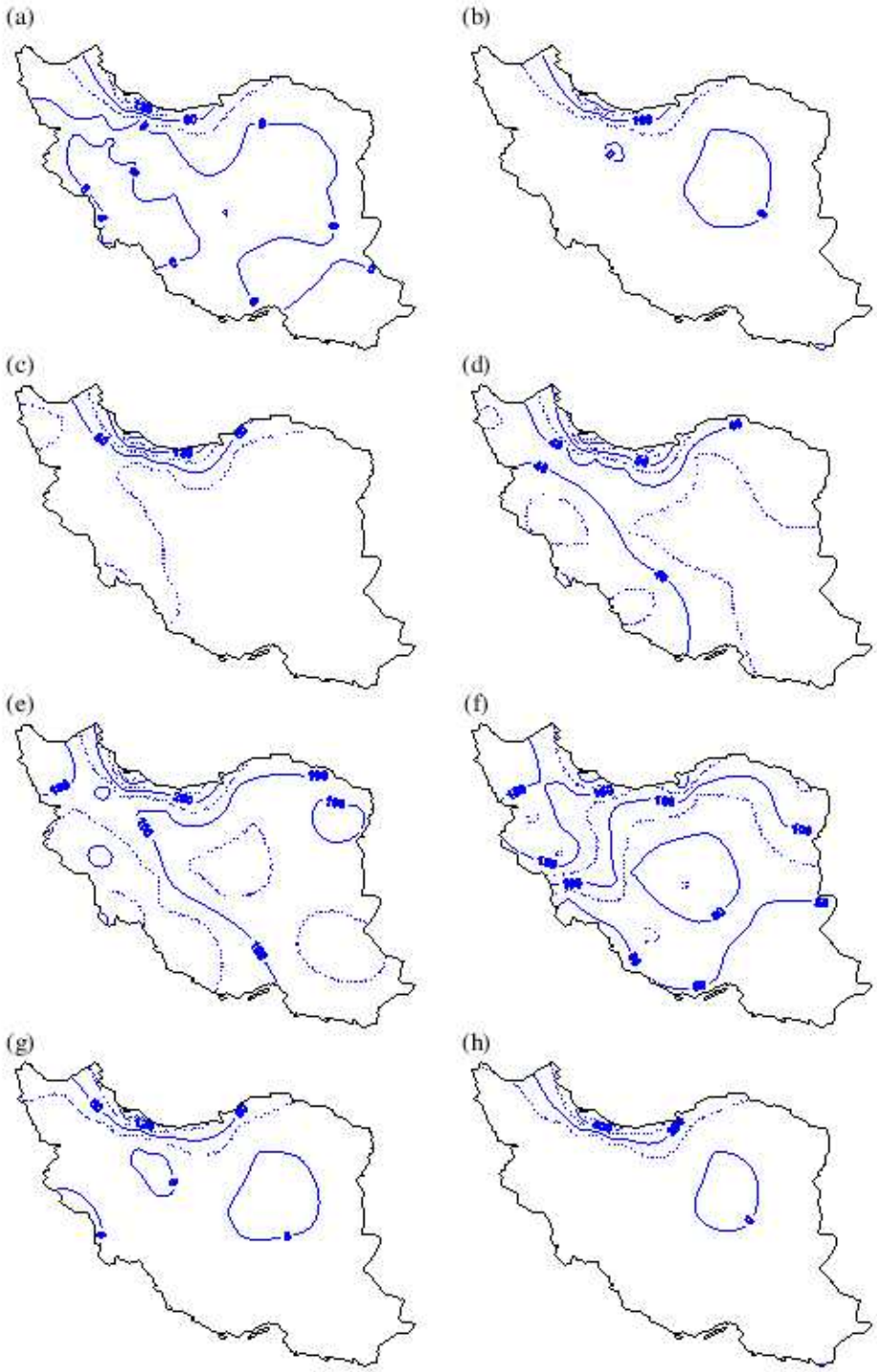

Figure 3. Average precipitation (mm) during 1960–2014 in Iran from September to December (a–d), and the seasons (e–h).

where $|\mathrm{WCS}_{i}(s)|$ and $\phi_i(s)$ denote the amplitude and the phase, respectively. Also, $\Im(\ldots)$ and $\Re(\ldots)$ represent the imaginary and real parts of a complex number, respectively. Larger $|\mathrm{WCS}_{i}(s)|$ means better correlation between two time series, while the $\phi_i(s)$ can be useful to delay detection of two time series (Liu, 1994; Torrence and Webster, 1999). Previous studies have shown that the WCS is not always reliable because it is not normalized, and it can reveal high WCS values when there is no actual time–frequency correlation between two time series (Maraun and Kurths, 2004). The WCO is a time-normalized and scale-resolved method to specify the correlation between two time series (Liu, 1994; Torrence and Webster, 1999; Grinsted *et al.*, 2004; Cazelles *et al.*, 2008):

$$\mathrm{WCO}_{i}(s) = \frac{\left| S\left\langle s^{-1}\,\mathrm{WCS}_{i}(s)\right\rangle\right|^{2}}{Ss^{-1}\left|W_{i}^{x}(s)\right|^{2}\,Ss^{-1}\left|W_{i}^{y}(s)\right|^{2}} \qquad (8)$$

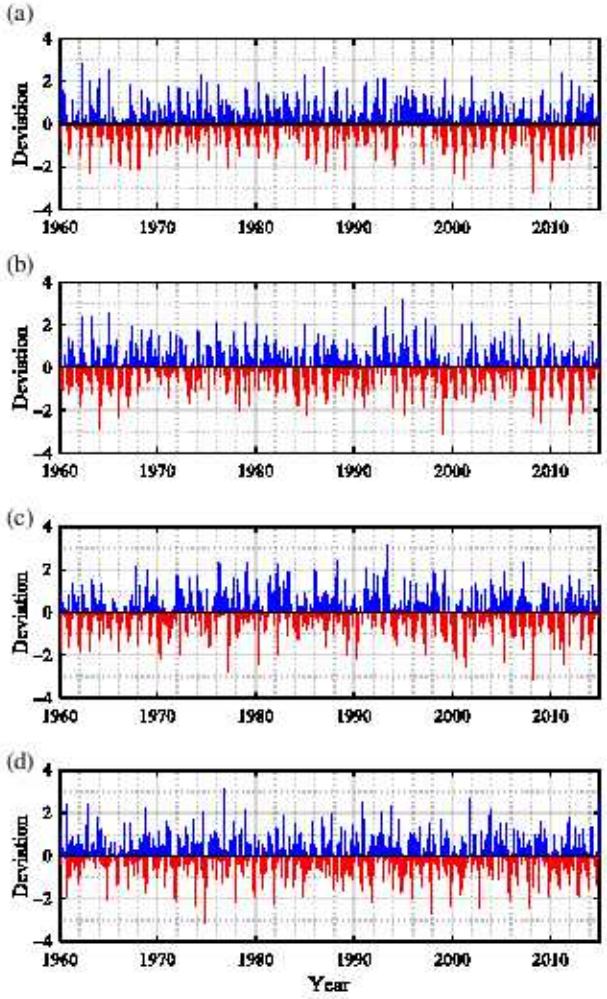

Figure 4. Standardized anomalies for the monthly precipitation (mm) time series in the stations of Kerman (a), Khorramabad (b), Mashhad (c) and Ramsar (d) for the period of 1960 to 2014.

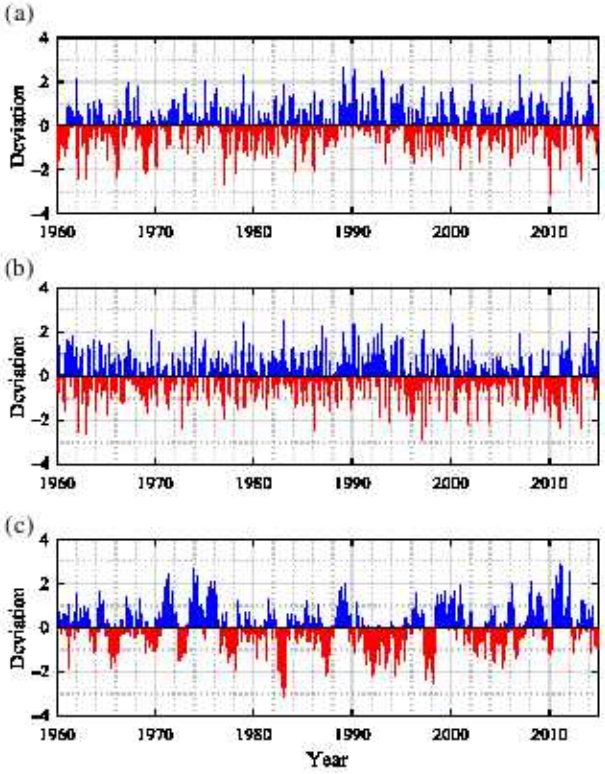

Figure 5. Standardized anomalies for the AO (a), NAO (b) and SOI (c) in the period of 1960–2014.

where $W_{I_i}^{x}(s)$ and $W_{I_i}^{y}(s)$ are WTs of two time series, $x(t)$ and $y(t)$, respectively, for the scale of s. The S letter in Equation (8) is the smoothing operator defined as follows (Grinsted *et al.*, 2004):

$$S(W) = S_{\text{scale}}\left(S_{\text{time}}\left(W_{I_i}(s)\right)\right) \tag{9}$$

where S_{scale} and S_{time} denote smoothing along the wavelet scale and time, respectively. Based on previous studies, a suitable smoothing operator for the Morlet wavelet can be seen in Equations (10) and (11) (Torrence and Compo, 1998; Torrence and Webster, 1999; Grinsted *et al.*, 2004; Brittain *et al.*, 2007).

$$S_{\text{time}}(W)\big|_s = \left(W_{I_i}(s)\ .\ c_1^{\frac{-t^2}{2s^2}}\right)\Big|_s \tag{10}$$

$$S_{\text{scale}}(W)\big|_t = \left(W_{I_i}(s)\ .\ c_2\Pi(0.6\,s)\right)\Big|_t \tag{11}$$

where the c_1 and c_2 are inserted in the above equations for the normalization process and are calculated numerically, and Π denotes the rectangle (box-car) function. It should be noted that the values of c_1 and c_2 have to be calculated for each normalization process, which is explained in detail in the previous studies (Torrence and Webster, 1999). It is clear that Equation (8) resembles the coefficient of determination equation, and therefore, the WCO has values ranging from 0 to 1 (Liu, 1994). For a better interpretation, one can compare the WPS, WCS and WCO to variance, covariance and coefficient of determination, respectively (Liu, 1994). The equations used for these correlation indices are analogies of one another, and are discussed and compared in more detail in Table 1 of Liu (1994). For analysis in a time space, variance, covariance and coefficient of determination can be the appropriate choices, while for analysis in a time–frequency space, the WPS, WCS and WCO are more appropriate. When the WCO is equal to 1, it can be interpreted as a perfect linear correlation between the two studied time series at the specific time (t_i) and scale (s), and when WCO is equal to zero, no correlation exists between $x(t_i)$ and $y(t_i)$, at the time t_i and scale s. The WCO is a more robust and trusty factor compared to the WCS (Maraun and Kurths, 2004; Gan *et al.*, 2007).

It should be noted that like many statistical methods, there is an uncertainty in the results obtained from the WCO method. The detected significant regions in the WCO plot are obtained with a 5% significance level, as the confidence level for most of the previous studies using WCO plots was taken to be 95%. Accordingly, one can conclude that the detected regions are correct at the 95% level, and this means that the obtained results could be incorrect, because of a 5% uncertainty level.

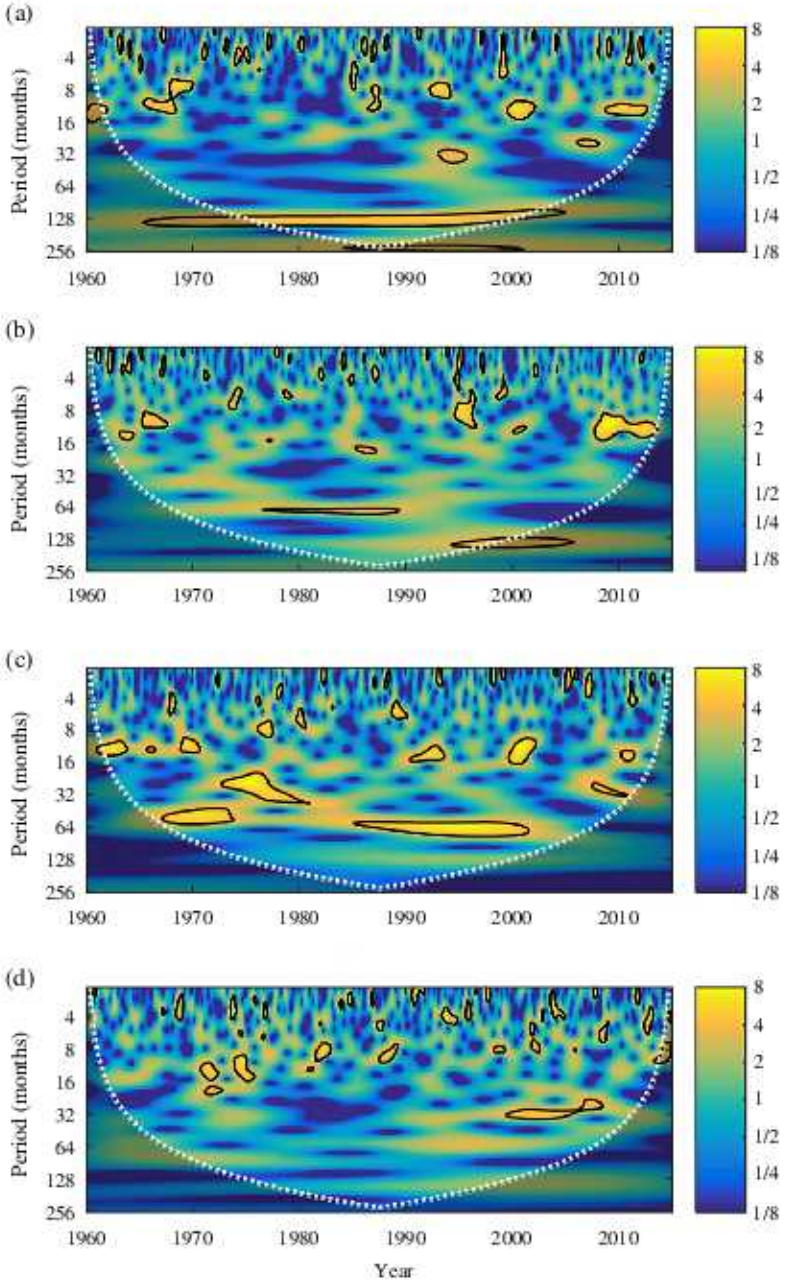

Figure 6. WPS for the monthly precipitation time series in the stations of Kerman (a), Khorramabad (b), Mashhad (c) and Ramsar (d) for the period of 1960–2014 (The regions with black thick outline present the 95% confidence level of local power, and the COI is specified with dotted white line and a transparent black fill).

The statistical significance of the wavelet power can be evaluated relative to the null hypothesis that the time series is stationary with a given background power spectrum (P_k). Generally, most of geophysical time series have red noise characteristics that can be modelled well by a lag-1 autoregressive (AR1) process. It should be noted that red noise has zero mean, constant variance, and is serially correlated in time, while white noise has zero mean, constant variance, but is uncorrelated in time. The power spectrum of an AR1 process can be calculated by:

$$P_k = \frac{1-\alpha^2}{\left|1-\alpha e^{-2i\pi k}\right|^2} \tag{12}$$

where α is lag-1 autocorrelation, and k is the Fourier frequency index. The theoretical distribution of the WCO of two time series with P_k^X and P_k^Y background power spectrums is given as (Torrence and Compo, 1998):

$$D\left(\frac{\left|W_{I_i}^X(s)\ W_{I_i}^Y(s)^*\right|}{\sigma_x\sigma_y} < p\right) = \frac{Z_v(p)}{v}\sqrt{P_k^X P_k^Y} \tag{13}$$

where $Z_v(p)$ is the confidence level related to the probability of p which can be obtained from a pdf defined by the square root of the product of two χ^2 distribution. For $v=1$ (real wavelets), $Z_1 = 2.182$, while for $v=2$ (complex wavelets), $Z_2 = 3.999$. Hence, the 5% significance level

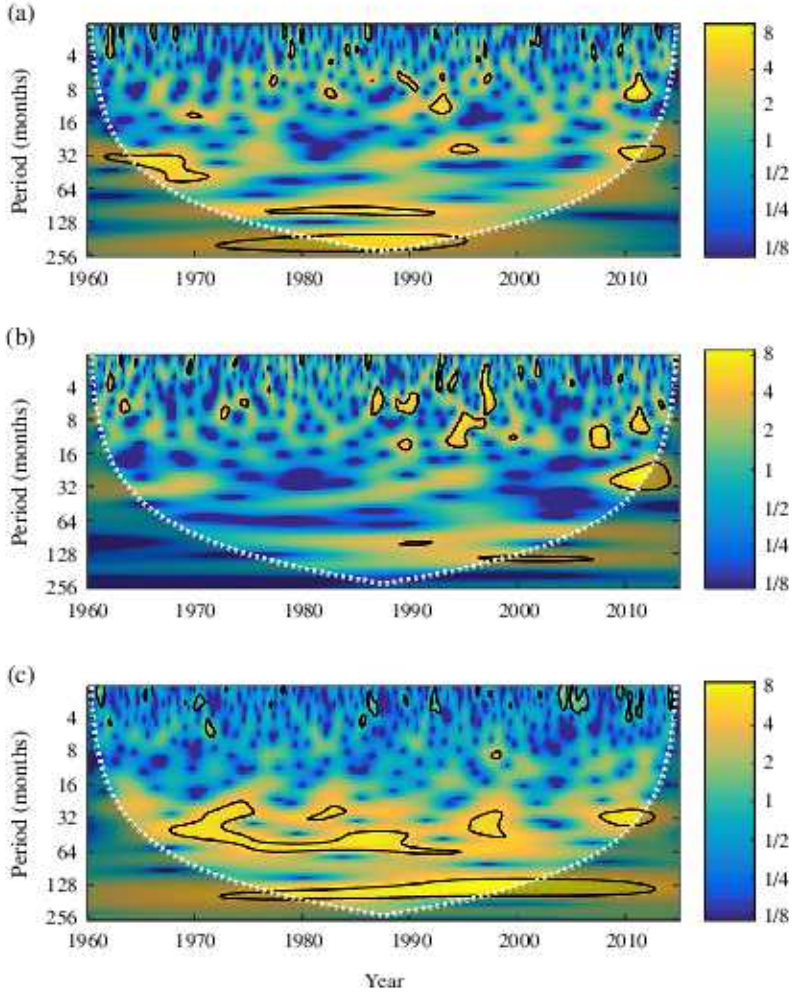

Figure 7. WPS for the AO (a), NAO (b) and SOI (c) time series for the period of 1960–2014 (The regions with black thick outline present the 95% confidence level of local power, and the COI is specified with dotted white line and a transparent black fill).

marked in the WCO plots is calculated using $Z_2 = 3.999$. The area of the 5% significance level can be interpreted by eye, and accordingly, the WCO is a visual interpreted method. The wider and larger area means a more continuous relationship between two time series in a specific frequency and time that these can be obtained from the WCO plot.

3. Data

3.1. Precipitation data

Iran is located between 44°E and 63°25′E longitude and 25°N and 38°39′N latitude in south west Asia and covers an area of approximately 1.65×10^6 km^2 (Araghi *et al.*, 2016). Based on the Köppen method, Iran has a semi-arid to arid climate, with the exception of the south coastlines of the Caspian Sea (Dinpashoh *et al.*, 2011). There are more than 200 synoptic stations across the country, but the length of data records at most of the stations is not sufficient, and they are therefore not appropriate for hydro-climatological studies (Maidment, 1993; Shelton, 2009). For this research, precipitation data was collected from 30 synoptic stations that are spatially dispersed in the country. These selected stations have the best quality data with the longest records (i.e. 50 years and more) of the 200 synoptic stations in Iran. Monthly precipitation data was obtained from the Iran Meteorological Organization (IRIMO) for the period of 1960–2014. The obtained data passed statistical quality tests such as the homogeneity and randomness test in the IRIMO data control unit. It should be noted that the central parts of the country (called the Central Desert and the Lut Desert) have a hyper arid climate with scant annual precipitation. These regions of the country have limited human inhabitance, and consequently there are only a few hydro-meteorological stations with insufficient data records in this region. The location and identification of the selected stations for this research are shown in Figure 1 and Table 1. Generally, precipitation in most regions of Iran usually occurs during mid-fall to mid-spring, but the southeastern part of the country is influenced by monsoon meteorological systems and precipitation in this region occasionally occurs in the summer. The north and west parts of the country receive more annual precipitation when compared to the east and south regions, and the minimum precipitation occurs in

Table 2. Dominant periods (except 12 months and shorter) and their occurrence years for precipitation during 1960–2014 in the studied stations.

Station name	Dominant periods (months)	Years of occurrence
Abadan	24; 60	(1972–1976) (1994–1999); (1985–1990)
Ahwaz	24; 60	(1994–1999); (1987–1995)
Arak	36-40	(1968–1976)
Babolsar	30-32	(1981–1984) (1997–2001) (2005–2011)
Bam	20-22	(2004–2010)
Bandar Abbas	–	–
Birjand	14–16; 20–34	(1999–2002); (2004–2011)
Bushehr	24; 28–32	(1993–2000); (1970–1973)
Esfahan	16; 32–40	(1978–1980) (1993–1995) (2006–2009); (1991–1997) (2005–2011)
Ghazvin	16; 18–32; 30–42	(2008–2012); (1994–2000); (1963–1973)
Gorgan	–	–
Hamedan	24; 32–50	(1984–1987); (1966–1975)
Kerman	32; 128	(1993–1995); (1976–2001)
Kermanshah	24–32	(1964–1973)
Khorramabad	64; 128	(1977–1990); (1994–2000)
Khoy	20-28;	(1984–1990)
Mashhad	18-36; 50–60; 62–80	(1973–1980); (1967–1974); (1985–2002)
Ramsar	28–34	(1999–2008)
Rasht	18–22	(1973–1976)
Sabzevar	30–48; 62–78	(1969–1975); (1987–2003)
Sanandaj	28-35; 70–90; 110–230	(1968–1972); (1969–1973); (1978–2001)
Shahrekord	32–48	(2003–2011)
Shahroud	12-32; 28–34; 32–40; 40–64	(1991–2002); (2008–2011); (1967–1974); (1986–1995)
Shiraz	16–20; 32–36; 36–48	(1993–1998); (1993–1997); (1965–1975)
Tabriz	16; 32–36; 64-80	(1981–1984); (1965–1967); (1987–1993)
Tehran	12–32; 32–48	(1994–2000); (1967–1972)
Torbat Heydarieh	12–24; 24–32; 64–80	(1993–2002); (1972–1974); (1991–2004)
Yazd	14–20; 16–32; 32–64	(1998–2001); (1974–1980); (1968–1974)
Zahedan	12–16; 16–32; 128	(1999–2004); (1994–1997) (2004–2009); (1987–1999)
Zanjan	32	(1968–1971) (1993–2001)

the central parts of Iran. Unfortunately, most of the synoptic stations in Iran do not have precipitation data with lengths greater than five decades. It should be noted that the local topography in the country has noticeable effects on precipitation amounts in the country, especially in the north and west parts of Iran. Two major mountain chains in the country, the Alborz and Zagros mountains, are located in the north and west parts of the country, respectively (see Figure 1). The Alborz mountains prevent the flow of humidity from the Caspian Sea to the central parts of the country, and therefore, coastal regions in the northern parts of Iran are categorized as having humid climates. Similarly, the western parts of the country have a relatively higher amount of precipitation, as the Zagros mountains prevent the flow of humidity to the central parts of Iran. Accordingly, the western Zagros has higher precipitation compared to the central and eastern parts of Iran. These issues with precipitation amounts in different regions of Iran are based on their regional climates , as the north, north western and western parts of the country have a more humid climate with higher amounts of precipitation compared to the other regions of Iran, and this is unrelated to large-scale climatic indices (see Figures 2 and 3).

3.2. Large-scale climatic indices

For this research, three climatic indices, namely the AO, NAO and SOI, were selected. The monthly time series for these indices were collected from the Climate Prediction Center and National Climatic Data Center, National Oceanic and Atmospheric Administration (http://www.cpc.ncep.noaa.gov, https://www.ncdc.noaa.gov) for the period of 1960–2014.

The AO is a large-scale pattern of climate variability also referred to as the Northern Hemisphere annular mode. The AO is characterized by winds circulating around the Arctic at a latitude of around 55°N. When the AO is in its positive phase, strong winds circulate around the North Pole and enclose colder air across the Polar Regions. These winds are weaker and less concentrated in the negative phase of the AO where the penetration of arctic air-masses in a southerly direction is easier, causing an increase in mid-latitude storms. The AO index is achieved by projecting the AO loading pattern to the anomaly of 1000-mb level or its equivalent, sea-level pressure (SLP) field over 20°–90°N latitude, and the loading pattern of the AO is defined as the leading mode of empirical orthogonal function analysis of the monthly mean SLP during the 1979–2000 period. The AO index was first identified by Edward Lorenz and later named by David Thompson and John Michael Wallace (Thompson and Wallace, 1998; Higgins *et al.*, 2000; Shelton, 2009).

The NAO is another well-known climatic teleconnection pattern in the Northern Hemisphere. The NAO represents the relative strength of the sea-level atmospheric

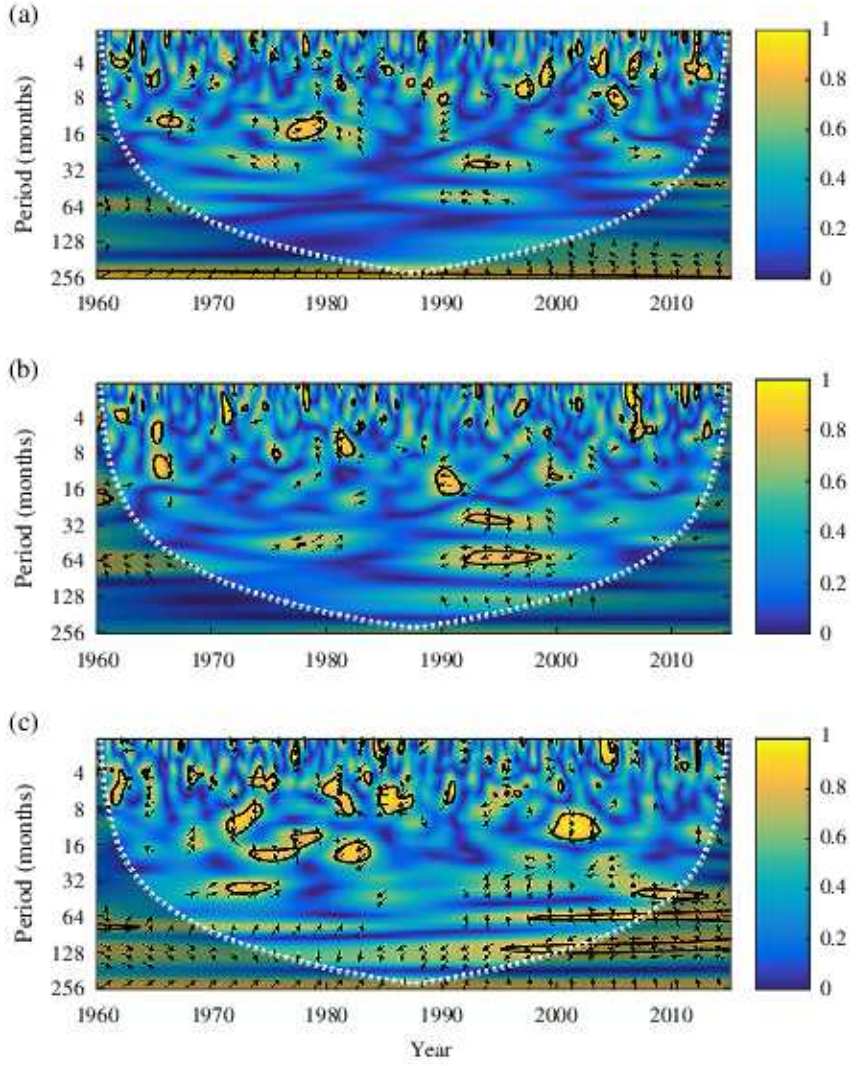

Figure 8. WCO and phase difference between precipitation in Kerman and the three studied climatic indices (i.e. AO (a), NAO (b) and SOI (c)). The 5% significance levels are specified with thick black contours. Arrows show the relative phase relationship between time series (right arrow: in-phase, left arrow: anti-phase).

pressure difference between the Akureyri, Icelandic low pressure centre located at 66°N, 18°W and the Ponta Delgada, Azores high pressure centre located at 38°N, 26°W. When both of these pressure centres are strong (weak), then the positive (negative) phase of the NAO occurs (Rogers, 1984; Jones *et al.*, 1997; Barry and Chorley, 2009). It should be noted that a strong pressure centre means a strong high (or low) pressure field, and accordingly, the positive (negative) phase of NAO occurs when the pressure gradient between these pressure centres is strong (weak). In the positive phase of the NAO, the westerlies (i.e. the winds which usually blow from the west in the mid-latitudes) are stronger, and accordingly, moist air is carried over Europe from the Atlantic Ocean. When the westerlies are strong, summers are cool, and winters are mild with frequent rainfall. Conversely, when the westerlies are weak, temperatures are higher in the summer and lower in the winter, leading to heat waves and deep freezes in addition to reduced precipitation (Hurrell and Van Loon, 1997; Jones *et al.*, 1997; Küçük *et al.*, 2009; Aguado and Burt, 2013). The NAO index was first identified by Wallace and Gutzler in the winter season (Wallace and Gutzler, 1981). The NAO has been widely used as a large-scale climate predictor for various hydro-climatological studies (Rogers, 1984; Hurrell and Van Loon, 1997; Yan *et al.*, 2004; Massei *et al.*, 2007; Massei *et al.*, 2010). It should be noted that although the AO and NAO have a close relationship and are in-phase most of the time, previous studies have revealed that the NAO may be more robust and relevant for climatic variabilities in the Northern Hemisphere, compared to the AO (Greatbatch, 2000; Ambaum *et al.*, 2001).

The SOI is a standardized climatic teleconnection index based on the mean sea level pressure differences between Tahiti at 18°S, 150°W, and Darwin, Australia, at 12°S, 130°E. The SOI in the most commonly used indicator for the ENSO. This atmospheric-oceanic circulation, first was identified by Sir Gilbert Walker in 1922 (Shelton, 2009). In general, the SOI time series corresponds well with the variations of ocean temperatures across the

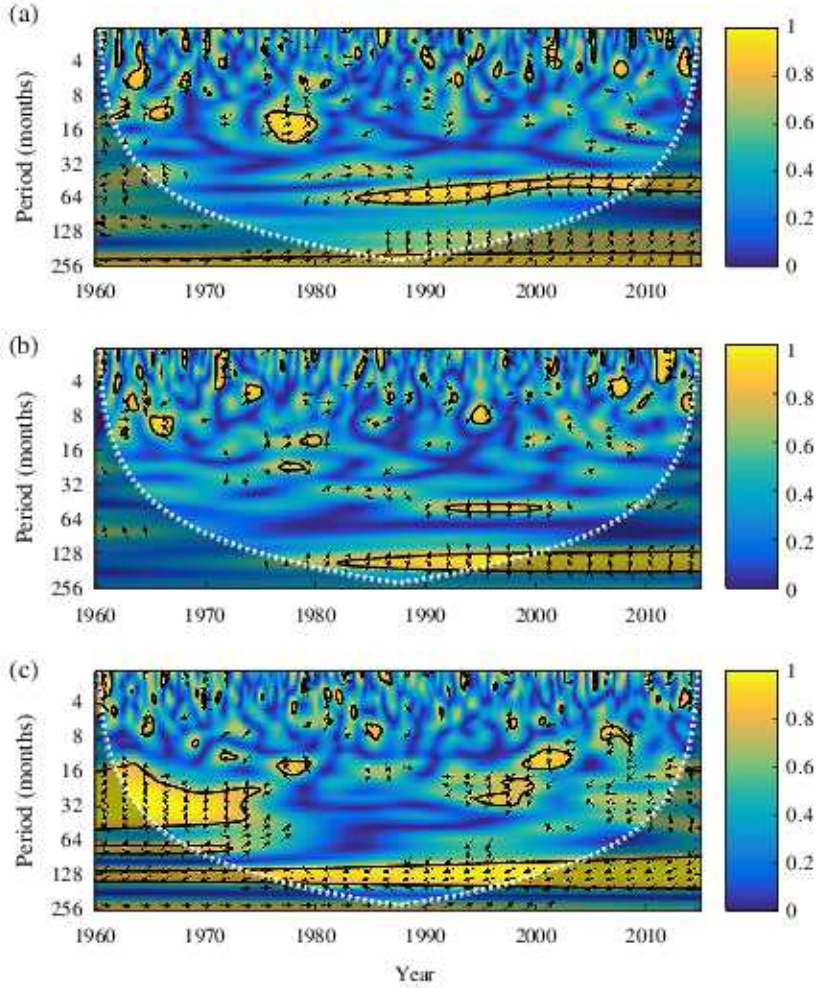

Figure 9. WCO and phase difference between precipitation in Khorramabad and the three studied climatic indices (i.e. AO (a), NAO (b) and SOI (c)). The 5% significance levels are specified with thick black contours. Arrows show the relative phase relationship between time series (right arrow: in-phase, left arrow: anti-phase).

eastern tropical Pacific (Bhalme and Jadhav, 1984). In the positive (negative) phase of the SOI, the strong easterly trade winds (low-level equatorial westerlies) flow over the central western Pacific Ocean. In the positive phase, which is called La Niña, waters in the central and eastern tropical Pacific Ocean become cooler than normal and the amount of precipitation over eastern and northern Australia generally increases. Contrariwise, in the negative phase, which is called El Niño, warmer waters are seen in the central and eastern tropical Pacific Ocean, and precipitation is less during winter and spring over the large parts of eastern Australia (Bhalme and Jadhav, 1984; Velasco and Mendoza, 2008; Barry and Chorley, 2009; Shelton, 2009).

The AO, NAO and SOI indices have been chosen for this research, because these three teleconnections are the most important and effective large-scale climatic patterns in the north and south hemispheres (Barry and Chorley, 2009; Shelton, 2009). Although, previous studies have shown that SOI has considerable effects on the climate of the north hemisphere as well (Bhalme and Jadhav, 1984; Liu *et al.*, 2005).

4. Methodology

In this research, the WCO was employed as the main method for studying the association between the precipitation in Iran and the three major climatic teleconnections (the AO, NAO and SOI). To achieve more detailed results, the time step for the data was not changed and the monthly time step was used. The following steps were taken for this study:

(1) The anomalies were calculated for the precipitation data employed in this study, based on the normal period, from 1961 to 1990. This normal period was recommended by the World Meteorological Organization for climatic studies (Von Storch and Zwiers, 1999; Wilks, 2011). These anomalies were standardized based on the Equation (14). (Montgomery and Runger, 2011). It should be noted that the times series for this study's indices were already standardized.

$$Z_{x_i} = \frac{x_{t_i} - \mu}{\sigma} \tag{14}$$

where μ and σ are the sample average and sample standard deviation of the time series $x(t)$, and the Z_{t_i} is the standardized x_{t_i}. Previous experiences with the WCO have shown

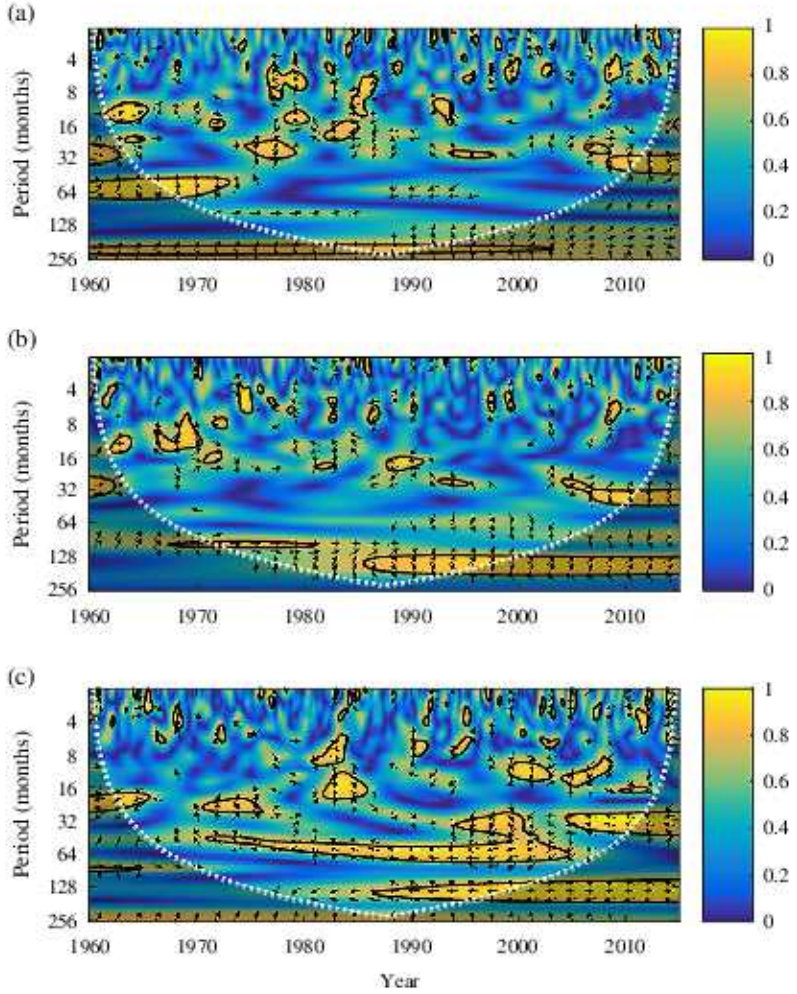

Figure 10. WCO and phase difference between precipitation in Mashhad and the three studied climatic indices (i.e. AO (a), NAO (b) and SOI (c)). The 5% significance levels are specified with thick black contours. Arrows show the relative phase relationship between time series (right arrow: in-phase, left arrow: anti-phase).

that using the main time series, instead of anomalies, and non-standardized series produces unreliable results, especially in geophysical and hydro-climatological data sets (Grinsted *et al.*, 2004; Maraun and Kurths, 2004; Jevrejeva *et al.*, 2005).

(2) The WPS was generated using Equation (4) for each time series, to determine the major predominant periods and their occurrence duration, based on the normalized time series obtained from applying Equation (14).

(3) The WCO was produced using Equation (8) for the precipitation data from each station and the selected climatic teleconnections. Using the WCO plot may reveal the relationship and the phase difference between each climatic teleconnection and precipitation at each station.

(4) It is always possible to find more than one predominant period via the WCO plots, for any two time series. In this research, the most effective predominant period was detected based on the duration. For example, if there are two significant regions in the WCO plot for the periods of 16 and 128 months, for which the duration of the first region is from 1970 to 1985 (i.e. 15 years), and the duration of the second region is from 1982 to 2006 (i.e. 24 years), then the 128-month period would be detected as the most effective and predominant period for this case, since it has the longer duration. This step was performed for each station separately and a spatial distribution report was produced on a base map of Iran for the results. Also, for the different climatic teleconnections (AO, NAO and SOI), each one with the longest significance region in the WCO plots is distinguished as the most important climatic index for precipitation in a particular station.

(5) For an overall conclusion for the whole country, the duration of each period (e.g. 4, 4–8, 8, 8–16, 16, 16–32, 32, 32–64, 64, 64–128, 128, 128–256) was summarized based on the duration values obtained for any station from the WCO plot based on the regions with 5% significance level. Finally, the percentage of each period was estimated for any of the studied teleconnections, and based on these calculated percentages, the most effective period for any teleconnection on the precipitation in Iran was detected. This was calculated as follows:

$$d_{P_i} = \sum_{j=1}^{m} d_{P_{ij}} \tag{15}$$

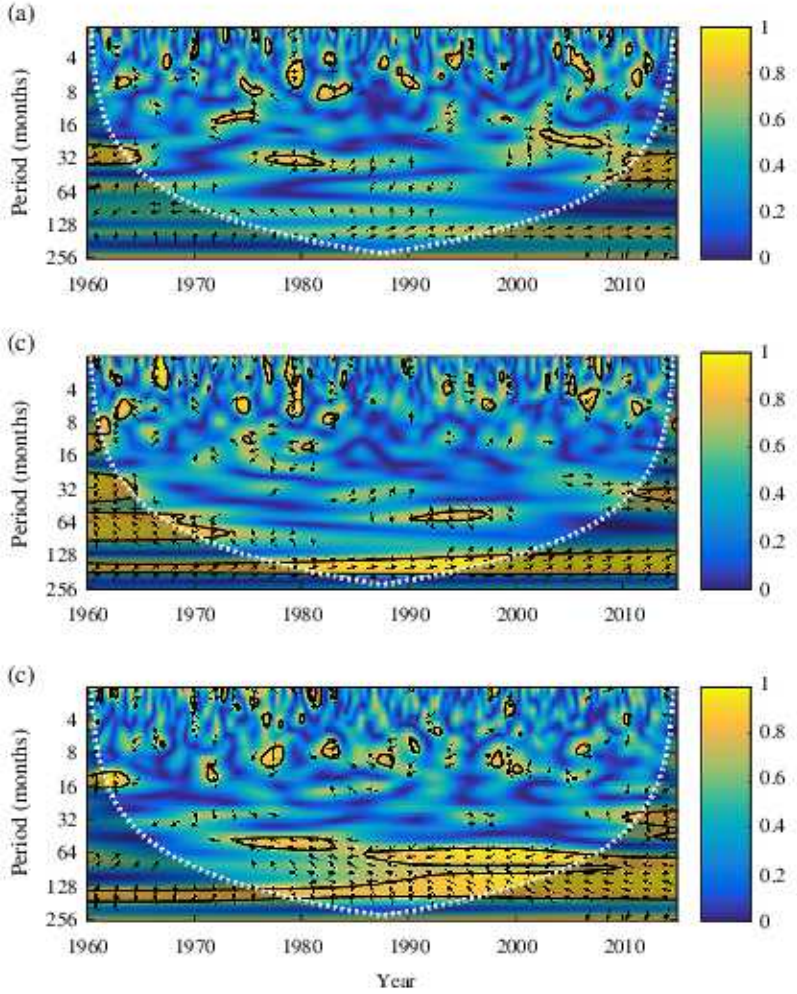

Figure 11. WCO and phase difference between precipitation in Ramsar and the three studied climatic indices (i.e. AO (a), NAO (b) and SOI (c)). The 5% significance levels are specified with thick black contours. Arrows show the relative phase relationship between time series (right arrow: in-phase, left arrow: anti-phase).

$$D_{\text{total}} = \sum_{i=1}^{n}\sum_{j=1}^{m} d_{p_{ij}} \tag{16}$$

$$\%p_i = \frac{d_{p_i}}{D_{\text{total}}} \tag{17}$$

where i and j are indicators for periods and stations, respectively, d_{p_i} denotes the duration of the region with a 5% significance level, for the p_i period. According to the criteria of this study, m (i.e. the number of stations) and n (i.e. the number of studied periods) had values equal to 30 (based on the explanations in Section 3.1) and 12 (based on the explanation in item 5 of Section 4), respectively. This last result was the country as a whole, in order to create an overall idea for future studies on the interactions of teleconnections and precipitation in Iran, in a time–frequency space.

5. Results and discussions

The standardized anomalies of the monthly precipitation and the three selected climatic teleconnections time series were calculated. For instance, the standardized anomalies for the monthly precipitation time series at the stations of Kerman, Khorramabad, Mashhad and Ramsar are shown in Figure 4. These stations are far from each other and have different climates. The standardized anomalies for the three climatic teleconnections are shown in Figure 5. To detect the dominant frequencies (or periods) in precipitation for each of the stations, the WPS was calculated for them all. For example, the WPS for the stations of Kerman, Khorramabad, Mashhad and Ramsar is shown in Figure 6. Also, the WPS is shown in Figure 7 for the AO, NAO and SOI.

Analyses of the WPS of monthly precipitation time series at all stations indicated that the 12-month or shorter predominant periodicity occasionally occurred in almost all of the stations during the studied period, which verified the natural variability of precipitation. In addition, other predominant periods, except 12 months or shorter, were observed in the precipitation WPS of the stations, but these frequencies were not dominant in the whole study period (1960–2014). These periodicities are shown in Table 2. Overall, some aspects can be interpreted from

Table 3. Results of WCO for the precipitation at the stations and the AO.

Station name	Duration	Period and phase difference (both in months)
Abadan	(1962–1965); (2007–2010); (1974–1981)	(8–16, in-phase); (32, anti-phase); (64–128, 3)
Ahwaz	(1962–1964); (1990–2010)	(8–16, in-phase); (32–64, anti-phase)
Arak	(1977–1982); (2007–2011); (1988–1995)	(16, in-phase); (16–32, 3); (64, 7.5)
Babolsar	(2008–2012); (1963–1968); (1997–2010); (1965–1972); (1984–1993)	(4–8, 10.5); (8–16, in-phase); (32–64, 3); (64, 3); (64, 7.5)
Bam	(1980–1995)	(128–256, 4.5)
Bandar Abbas	(1978–1995)	(128–256, 3)
Birjand	(1980–1995)	(128–256, 3)
Bushehr	(1962–1966)	(8–16, in-phase)
Esfahan	(1962–1967)	(8–16, 3)
Ghazvin	(1962–1973); (1998–2005)	(16–32, anti-phase); (64, anti-phase)
Gorgan	(1998–2010); (1965–1972); (1985–2005)	(32, 3); (64, 4.5); (64, 9)
Hamedan	(1988–1992); (1994–2004)	(64, anti-phase); (64–128, 4.5)
Kerman	(1977–1980)	(16, 1.5)
Kermanshah	(1965–1970); (2001–2010)	(32, anti-phase); (32–64, anti-phase)
Khorramabad	(1976–1980); (1983–2010)	(16, 1.5); (32–64, 7.5)
Khoy	(1963–1970); (1967–1973); (1986–1992)	(32, anti-phase); (64, 3); (64, 7.5)
Mashhad	(1965–1972)	(64, 3)
Ramsar	(2002–2008)	(16–32, in-phase)
Rasht	(1972–1993); (1980–1995)	(128, 3); (128–256, in-phase)
Sabzevar	(1975–1983); (1965–1973); (1988–1993)	(16, 3); (64, 3); (64, anti-phase)
Sanandaj	(1965–1972); (1985–1995)	(64, 4.5); (64, 9)
Shahrekord	(1975–1980); (1985–1995)	(16, 1.5); (64, anti-phase)
Shahroud	(2008–2011); (1985–1995); (1972–1981); (1982–1999)	(32, 3); (64, anti-phase); (64–128, in-phase); (128–256, 1.5)
Shiraz	(1966–1980)	(32–64, 3)
Tabriz	(2005–2011); (1965–1970); (2002–2007); (1984–2000);	(16, 7.5); (32, anti-phase); (32, 1.5); (64, 9)
Tehran	(2005–2010); (1982–1994)	(32, 3); (64, 7.5)
Torbat Heydarieh	(1992–1998); (2008–2010); (1966–1972); (1983–1990)	(32, 4.5); (32–64, 3); (64, 3); (64, anti-phase)
Yazd	(1964–1970); (1968–1978); (1990–1996); (2002–2006); (1972–2000)	(8–16, 1.5); (32–64, 1.5); (32–64, 4.5); (64, 3); (64–128, 3)
Zahedan	(1992–1995); (1989–1998)	(8–16, 7.5); (64, 3)
Zanjan	(1978–1980); (1965–1970); (2007–2010)	(8, 3); (32, anti-phase); (32, 3)

Table 2: first, detecting the predominant periodicities and years of occurrence is not an easy procedure by visual inference alone; second, it is clear that long-term periodicities have longer durations in the time series; third, it can be seen that stations with arid and semi-arid climates (e.g. Esfahan, Kerman, Mashhad, Sabzevar, etc.) usually have more long-term periodicities, compared to the stations with humid or semi-humid climates (e.g. Bandar Abbas, Gorgan, Rasht, etc.), but this is not an absolute rule for all stations. The WPS of the AO, NAO and SOI are shown in Figure 7. As can be in this figure, the AO has longer term predominant periodicities compared to the NAO, while the maximum dominant period of the NAO is 16 to 32 months of fluctuation, which occurred from around 2008 to 2012. The WPS of the AO revealed that the 32- to 64-month periods occurred from 1965 to 1972, and 2009 to 2010. Likewise, the 64- to 128-month periods were observed only from 1977 to 1992, and a longer term period with a 128- to 256-month fluctuation was sharp only during 1980–1990, for the AO time series. The WPS of the third climatic teleconnection, the SOI, was relatively different from the other climatic indices studied. It seemed that the SOI had a more continuous fluctuation pattern compared to the AO and NAO. As can be seen in Figure 7, there was a continuous region with a 32- to 64-month period during 1967–1995, while there were some dispersed regions with a 32-month period that occurred during 1980–1983, 1996–2000, and 2008–2010. In addition, a long-term frequency with a 128- to 256-month period was seen from 1976 to 2004.

To find the association between precipitation in Iran and the selected large-scale climatic indices, the WCO was calculated for every studied station. For instance, the WCO plots for Kerman, Khorramabad, Mashhad, and Ramsar stations are shown in Figures 6–9. For the Kerman station, it seemed that there was no noticeable relationship between precipitation and the AO, since most of the regions with a 5% significance level were very small and scattered. Similarly, the relationship between the NAO and precipitation at the Kerman station was not very perceptible, since there was only a significant 64-month period area from 1992 to 1998, in which the precipitation and the NAO were in an anti-phase mode. The maximum number of regions with a 5% significance level were observed in the WCO of precipitation and the SOI at the Kerman station (see Figure 8), as these regions have more continuity compared to the that of significant areas in the

Table 4. Results of WCO for the precipitation at the stations and the NAO.

Station name	Duration	Period and phase difference (both in months)
Abadan	(1988–1991)	(8–16, anti-phase)
Ahwaz	–	–
Arak	(1991–2003); (1980–2000)	(32–64, 7.5); (128–256; 3)
Babolsar	(2007–2012); (1981–1988); (1990–1996); (1994–2005)	(8, in-phase); (64, 9); (64, 9); (64–128, 7.5)
Bam	(1989–1991); (2007–2009); (1997–2005)	(8–16, anti-phase); (8–16, 9); (64–128, 9)
Bandar Abbas	(1995–1997); (1994–2001)	(8–16, anti-phase); (64, anti-phase)
Birjand	(1988–1990)	(16, 7.5)
Bushehr	(1962–1964); (1976–1981); (1989–1994)	(8–16, in-phase); (8–16, 10.5); (8–16, anti-phase)
Esfahan	(1974–1981)	(32–64, 3)
Ghazvin	(1962–1969)	(32, anti-phase)
Gorgan	(2004–2009)	(32, 1.5)
Hamedan	(1965–1968); (1988–2005)	(32, anti-phase); (64–128, 4.5)
Kerman	(1992–1998)	(64, anti-phase)
Kermanshah	(1965–1975); (1991–2000)	(32–64, anti-phase); (32–64, 9)
Khorramabad	(1992–2000); (1982–2000)	(64, 9); (128–256, 3)
Khoy	(1963–1969); (1980–2000)	(32–64, anti-phase); (128–256, 3)
Mashhad	(1967–1970); (2003–2010); (1972–1981); (1986–1999)	(8–16, 3); (32, 3); (64–128, in-phase); (128–256, 3)
Ramsar	(1979–1980); (1990–1997); (1966–1972)	(4–8, in-phase); (64, 10.5); (128–256, in-phase)
Rasht	(1985–1990); (2009–2011); (1970–1990); (1990–1998)	(4–8, in-phase); (16–32, in-phase); (64–128, 1.5); (128, in-phase)
Sabzevar	(1965–1970); (1971–1977); (1987–1990); (1994–1999)	(8–16, 3); (16, 1.5); (16–32, 7.5); (64, 9)
Sanandaj	(1993–1997); (1963–1974); (1984–1990); (1980–2000)	(4–8, 9); (32, 9); (128, 4.5); (128–256, 4.5)
Shahrekord	(1975–1980); (1985–1997)	(16–32, in-phase); (128–256, 1.5)
Shahroud	(1977–1998)	(128, 1.5)
Shiraz	(1965–1967); (1972–1976); (1967–1973)	(8–16, 3); (8–16, 7.5); (32, 9)
Tabriz	(1968–1972); (1989–1991); (1965–1971); (1995–2000); (1980–1998)	(8–16, 4.5); (16, 7.5); (32–64, anti-phase); (64, 10.5); (128, 3)
Tehran	(1972–1975); (2005–2010); (1971–1987)	(4–8, 1.5); (32, 3); (64–128, 4.5)
Torbat Heydarieh	(1967–1970); (2003–2010)	(8–16, 3); (32, 3)
Yazd	(1993–1997); (1985–1990); (1972–1995)	(8–16, anti-phase); (16–32, anti-phase); (128, 3)
Zahedan	(1982–1991); (2000–2003); (1995–2000); (1984–1999)	(8–16, anti-phase); (8–16, anti-phase); (32–64, 4.5); (128–256; 4.5)
Zanjan	(1977–1980); (2006–2011); (1964–1972); (1974–1988)	(8, 4.5); (16–32, 1.5); (32–64, 7.5); (128, 3)

WCO of the AO and the NAO. The phase difference in any of the mentioned WCO plots did not have a uniform status. For the station of Khorramabad, it was observed that the AO was more effective, compared to the station of Kerman (see Figure 9). In the WCO plot for Khorramabad and the AO, there was a 5% significant region with a 16-month period from 1976 to 1980, and a larger significant region from 1983 to 2010 with a 32- to 64-month period. For the NAO index, relatively large significant areas in the WCO were observed. For the SOI, the WCO plot for the Khorramabad station showed that significant areas were larger compared to the WCO plots for the AO and NAO. Thus, it can be interpreted that the SOI was the most effective climatic teleconnection for this station, as well as the station of Kerman. For the station of Mashhad, similar to the other two stations, it can be interpreted that the SOI was the most effective climatic teleconnection index on precipitation (see Figure 10). Most of the areas with a 5% significance level were scattered and relatively small in the WCO plots for the AO and NAO in the Mashhad station, while in the WCO plot for the SOI, the significant areas were approximately continuous with a uniform phase difference in which the precipitation and the SOI were anti-phase most of the time. In a similar status, for the station of Ramsar, the SOI and the NAO were the most effective large-scale climatic indices, respectively. The largest significant region for the NAO was observed in the 128- to 256-month period section in the WCO, with an in-phase status (see Figure 11). For the SOI, the 5% significant areas were larger, compared to the WCO for the AO and NAO, and significant regions with a 64- to 128-month period were observed for the SOI and the precipitation at the Ramsar station.

The most predominant periods, phase difference and occurrence duration for the regions with a 5% significance level (in the WCO plots) were detected and are listed for all of the studied stations in Tables 3–5. From these tables, it can be interpreted that the SOI was the most effective climatic teleconnection for the precipitation at most of the stations, since the longest durations for the 5% significance level regions were detected in the WCOs for the SOI and precipitation. As obtained in India, the

Table 5. Results of WCO for the precipitation at the stations and the SOI.

Station name	Duration	Period and phase difference (both in months)
Abadan	(1990–2000); (1965–1980); (1980–1990); (2006–2010); (1992–2001)	(32, 9); (32–64, 3); (32–64, 4.5); (32–64, 7.5); (128, 7.5)
Ahwaz	(1980–1983); (1963–1982); (1994–1999); (1968–1975); (1988–1997); (1992–2000)	(4, 1.5); (16–32, 3); (32, 7.5); (64, 1.5); (64, anti-phase); (128; anti-phase)
Arak	(1975–1980); (1970–1975); (2008–2011); (1965–1976); (1978–2002)	(16, 4.5); (16–32, 3); (32, anti-phase); (32–64, 3); (128–256, anti-phase)
Babolsar	(1981–1985); (1962–1968); (1973–1981); (1995–2012)	(16, 10.5); (16–32, anti-phase); (16–32, 1.5); (16–32, anti-phase)
Bam	(2000–2009); (1963–1966); (1983–1985); (1970–1978);	(8–16, 9); (16–32, 7.5); (64, anti-phase); (64–128, 3)
Bandar Abbas	(2000–2005); (1990–1998); (1974–1979); (1995–2001)	(8–16, 9); (16, anti-phase); (16–32, 1.5); (32, 7.5)
Birjand	(2000–2005); (2008–2012); (1963–1966); (1970–1974); (1983–2008); (2007–2010)	(8–16, 9); (16, 9); (16–32, 7.5); (16–32, 3); (64, anti-phase); (32–64, anti-phase)
Bushehr	(1965–1985); (1992–2006)	(32–64, 3); (64, 4.5)
Esfahan	(1992–1997); (1965–1980); (2005–2011); (1994–2003); (1990–2000)	(16, anti-phase); (32, 3); (32, anti-phase); (64, anti-phase); (128, anti-phase)
Ghazvin	(2007–2012); (1997–2002); (1963–1975); (1990–1995); (2008–2010)	(8–16, 7.5); (16–32, 7.5); (32–64, 4.5); (32, 9); (32, anti-phase)
Gorgan	(1975–1978); (1964–1966); (1993–2010); (1984–1992)	(16–32, 3); (32, anti-phase); (16–32, anti-phase); (64, 9)
Hamedan	(1962–1964); (1999–2002); (1990–2000); (1964–1975); (1985–2000)	(8–16, 3); (8–16, 9); (16–32, 7.5); (32–64, 3); (128, 7.5)
Kerman	(1980–1982); (1986–1989); (1970–1973); (2000–2003); (1972–1980); (1981–1983); (1972–1974); (1997–2007); (1995–2002)	(4–8, 4.5); (8, anti-phase); (8–16, 3); (8–16, 9); (16, 4.5); (16, anti-phase); (32, in-phase); (64, 4.5); (128, 7.5)
Kermanshah	(1990–1996); (1970–1974); (1968–1973); (1988–2000)	(16, 7.5); (16–32, 3); (64, in-phase); (128, anti-phase)
Khorramabad	(1998–2002); (1962–1973); (1995–2000); (1975–2002)	(8–16, 9); (16–32, 3); (16–32, 7.5); (128, anti-phase)
Khoy	(2008–2012); (1995–1997); (2004–2010); (1993–2006); (1976–2004)	(16, 7.5); (32, 3); (32, 7.5); (64, 7.5); (128–256, anti-phase)
Mashhad	(1980–1983); (1998–2008); (1982–1985); (1962–1965); (1970–1976); (1970–2011); (1988–2000)	(8, in-phase); (8–16, 9); (16, 9); (16–32, anti-phase); (16–32, 3); (32–64, anti-phase); (128, anti-phase)
Ramsar	(1974–1983); (1986–2007); (1976–2004)	(64, anti-phase); (64, anti-phase); (128, 4.5)
Rasht	(2002–2011); (1992–2004)	(16–32, anti-phase); (128, 4.5)
Sabzevar	(2008–2012); (1971–1975); (1979–1983); (1990–2001); (1968–1976); (1988–2001)	(8–16, 7.5); (16–32, 3); (32, 1.5); (32, 9); (32–64, 3); (64, anti-phase)
Sanandaj	(1996–2004); (1997–2000); (1965–1975); (2005–2010); (1995–2002); (1975–2002)	(8–16, 7.5); (16–32, 7.5); (16–32, 3); (32, anti-phase); (32–64, anti-phase); (128–256, 7.5)
Shahrekord	(1975–1980); (1990–1995); (1967–1971); (1995–2000); (2004–2011); (1990–2000)	(16, anti-phase); (16, anti-phase); (32, 4.5); (32, 9); (32–64, anti-phase); (64, anti-phase)
Shahroud	(1971–1973); (1996–2002); (1963–1978); (1991–2002); (2007–2011); (1990–1998)	(8, 4.5); (8–16, 9); (16–32, 4.5); (16–32, 9); (32, anti-phase); (64, anti-phase)
Shiraz	(1965–1976); (1996–2000); (2008–2010)	(32–64, 4.5); (32, 9); (32, anti-phase)
Tabriz	(1998–2002); (1995–2001); (2010–2012); (2005–2010); (1972–1976); (1978–2000)	(4–8, in-phase); (8–16, 9); (16, anti-phase); (32, anti-phase); (32–64, 4.5); (128–256, anti-phase)
Tehran	(1988–1992); (2008–2011); (1964–1978); (1990–2000); (2005–2011); (1990–1999); (1992–2001)	(4–8, 4.5); (8–16, 9); (16–32, 4.5); (32, 9); (32, anti-phase); (64, anti-phase); (128, anti-phase)
Torbat Heydarieh	(1983–1985); (2000–2003); (2006–2009); (1970–1983); (1995–2011); (1992–1998)	(4–8, in-phase); (8–16, 9); (8–16, 7.5); (16–32, 3); (16–32, anti-phase); (64, anti-phase)
Yazd	(1980–1983); (1997–2008); (1964–1973); (1980–1999)	(4–8, in-phase); (8–16, 9); (32–64, 3); (64, 4.5)
Zahedan	(1965–1967); (1989–1991); (2000–2004); (2003–2005); (1970–1993); (1978–2000)	(4–8, 3); (4–8, in-phase); (8–16, 9); (16–32, anti-phase); (64, 3); (128, 9)
Zanjan	(1998–2001); (2008–2011); (1976–2000)	(16–32, 7.5); (16–32, anti-phase); (128–256, 7.5)

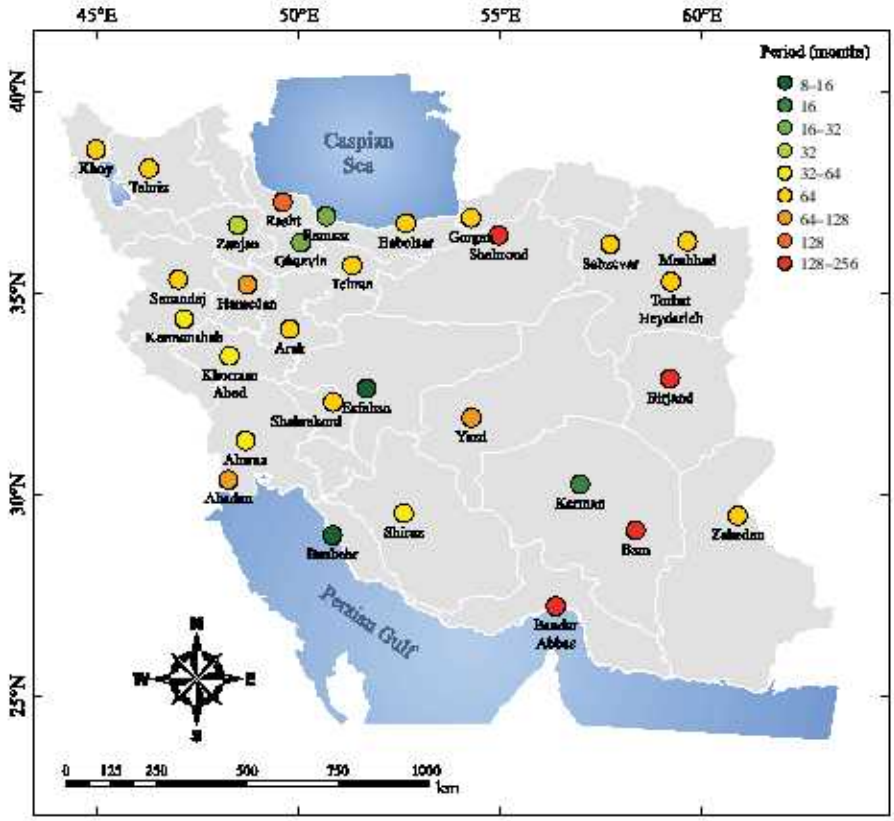

Figure 12. Predominant periods obtained from the WCO plot of the AO and precipitation.

SOI has a positive and highly significant relationship with the Indian monsoon in different seasons for the period 1871–1978 (Mooley *et al.*, 1985). A study in Nepal showed that the influences of the SOI are very significant for Nepal's monsoon, since when the SOI is in a negative (positive) phase, rainfall is lower (higher) than the normal values (Shrestha, 2000). As seen in previous studies in Turkey, the SOI phases play major roles in the Turkish and the eastern Mediterranean regions' precipitation, even when the SOI is in the extreme phase (Çağatay Karabörk and Kahya, 2003, 2009). It seems that the SOI plays a major role in the precipitation amount and occurrence in this region, and the previous studies agree with the main results of this research. Tables 3–5 are applicable for detailed information about effective periodicities and phase differences that were detected between the AO, NAO and SOI and the precipitation at the individual stations.

For an overall interpretation, the most effective period at each station and each of the climatic teleconnections was found based on the time duration of that periodicity. For example, in the station of Rasht, the WCO plot for the NAO detected four regions with a 5% significance level (see Table 4), while the region with a 64- to 128-month period had the longest duration compared to the other significant regions, and therefore this period (i.e. 64–128 months) was selected as the most dominant and effective period between the NAO and precipitation at the Rasht station. This procedure was performed for all of the stations and every studied climatic index. The final results are shown in Figures 10–12. For the AO index, it was observed that only six stations (Bushehr, Esfahan, Kerman, Ramsar, Rasht and Zanjan) had predominant periods equal to or less than 32 months, and the other stations had longer term periods, especially equal to or greater than 32 months (see Figure 12). For the NAO index, the predominant periods for most of the studied stations were equal to or greater than 64 months, although at around 27% of the stations, the predominant period was 32 months or less (see Figure 13). The most noticeable spatial pattern was observed for the SOI, since the longer term periods belonged to the western and northwestern stations, with periods of more than 64 months (see Figure 14). For the SOI, the predominant periods of less than 64 months were observed in all parts of the country, except for the northwestern regions. In Figure 15, the average percentages of each period for all of the studied climatic indices in Iran are presented. As can be that for the AO and SOI, the distribution was near to normal, while for the NAO the longer term periods were more effective (see Figure 15). For the AO, the 64-month period was the most effective and predominant period, while for the NAO, the 128- to 256-month period was dominant. For the SOI, distribution was relatively normal and the middle classes were the most dominant periods. For the phase difference, a uniform distribution was not observed as it had a random pattern most of the time, although in some cases (e.g. long-term periods in the SOI), the anti-phase was detected at most of the stations. As can be seen in the results of this research, the SOI has stronger effects on precipitation in Iran, similar to the results obtained in neighbouring countries such as India, Nepal and Turkey

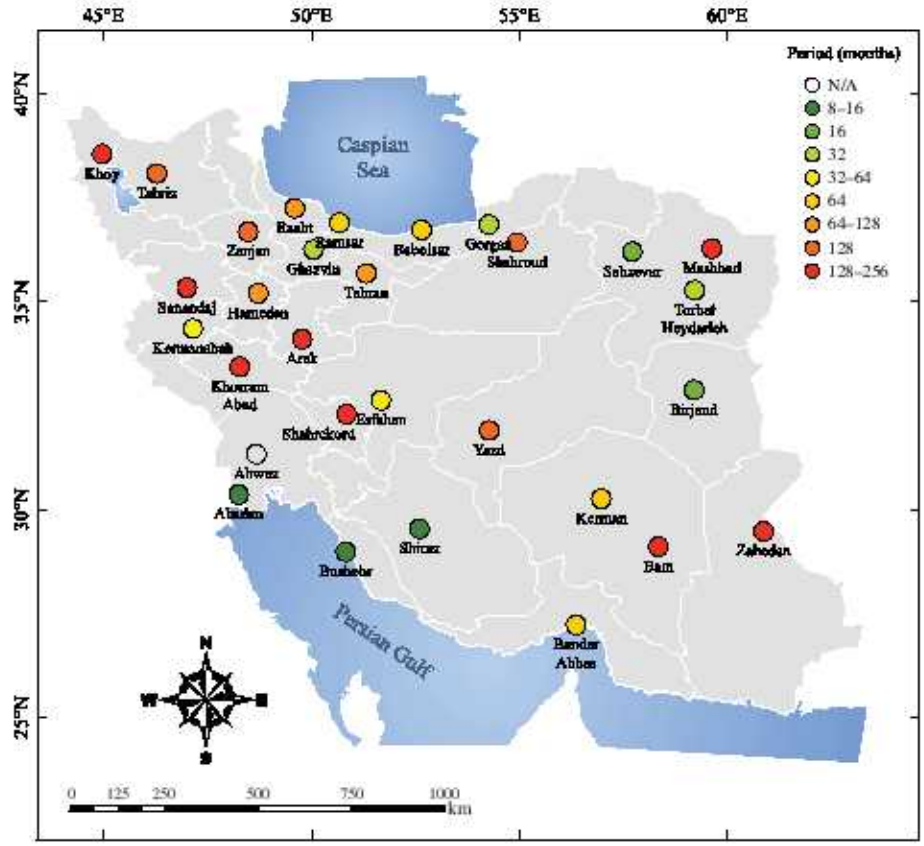

Figure 13. Predominant periods obtained from the WCO plot of the NAO and precipitation.

(Mooley *et al.*, 1985; Shrestha, 2000; Çağatay Karabörk and Kahya, 2003, 2009). It seems that the climatic indices which are derived from sea surface temperature, such as the SOI, have more noticeable influences on the precipitation in this region compared to the climatic indices which are based on pressure systems, such as NAO, and this result is in agreement with previous studies in neighbouring regions (Çağatay Karabörk and Kahya, 2003, 2009).

These six stations are not located in a specific region of the country, but they are spread more in the north and west parts of Iran. Accordingly, it can be concluded that the periods rise when the longitude increases from west to east. For instance, the longest periods are observed in the eastern stations, such as Birjand, Bam, etc., while the shortest periods are observed more in the western parts of the country (see Figure 12). It is clear that a denser network of meteorological stations would improve the results of this study, but unfortunately the lack of weather stations, especially in the central and southeastern parts of the country, affects the results. As can be seen in Figure 13, the longest periods are observed more in the west and north west parts of the country, while the shortest periods are observed in the south west regions, for instance, in the stations of Abadan, Bushehr and Shiraz. In addition, shorter periods are observed in the north east part of Iran, for example, in the stations of Sabzevar, Torbat Heydarieh and Birjand, while the station of Mashhad shows the longest period (i.e. 128 to 256 months). This could be an interesting topic for further studies to explore why this occurred. One possible hypothesis is the effects of heat islands on the precipitation amount and intensity, but this issue needs more detailed studies. Overall, it seems that the pattern observed for effective periods of the NAO in Iran is more regular compared to the patterns observed for the AO in Figure 12. As can be seen in Figure 14, the longest periods are observed in the northwestern part of the country, at stations such as Khoy, Tabriz, Zanjan, etc., while the shortest periods are detected in the southeastern and northeastern parts of Iran. It seems that precipitation and the SOI are correlated with shorter periods in the central and eastern regions of the country, and it is interesting that most of these regions have an arid or semi-arid climate, compared to the north and northwestern parts of Iran, which have semi-arid to humid climates. It can be concluded that precipitation amounts in the central and eastern regions of Iran are affected within shorter durations by the SOI variations. The precipitation in these regions (i.e. central and eastern parts) occurs mostly in the winter, and it is expected that the SOI variations influence the amount of precipitation in the central and eastern parts of the country in the winter more so than in other seasons.

The obtained results had relatively good conformity with the major periodicities of the studied large-scale circulations. For instance, based on previous studies, the NAO has major peak centres at 2.1, 8 and 24 years (Cook *et al.*, 1998; Anctil and Coulibaly, 2004), and the results of this study showed that these peaks are the main effective predominant periodicities for precipitation in

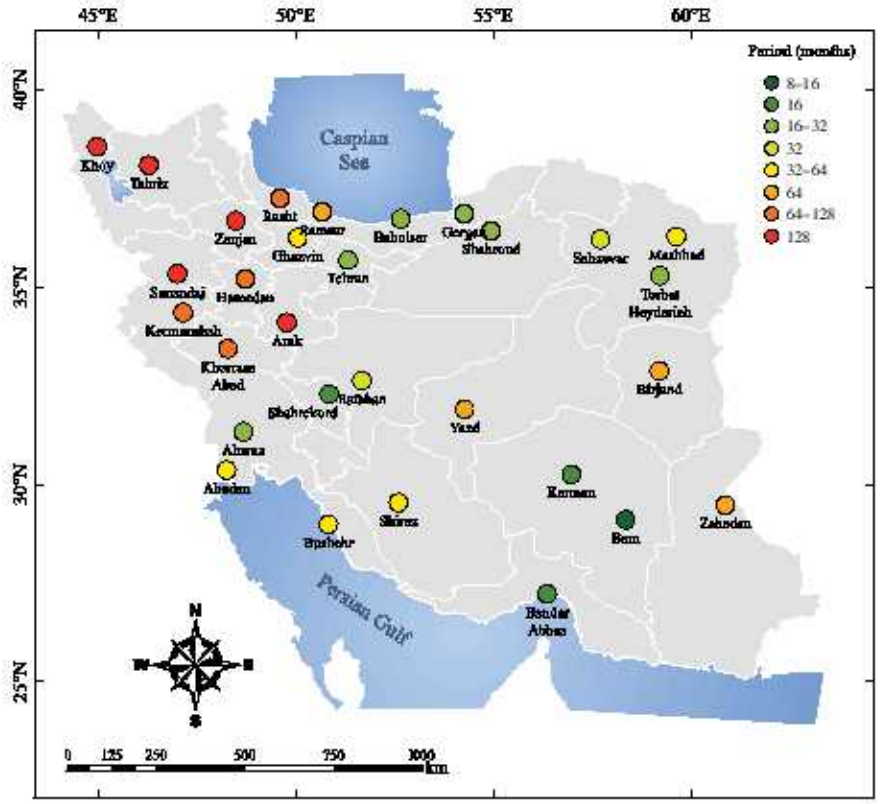

Figure 14. Predominant periods obtained from the WCO plot of the SOI and precipitation.

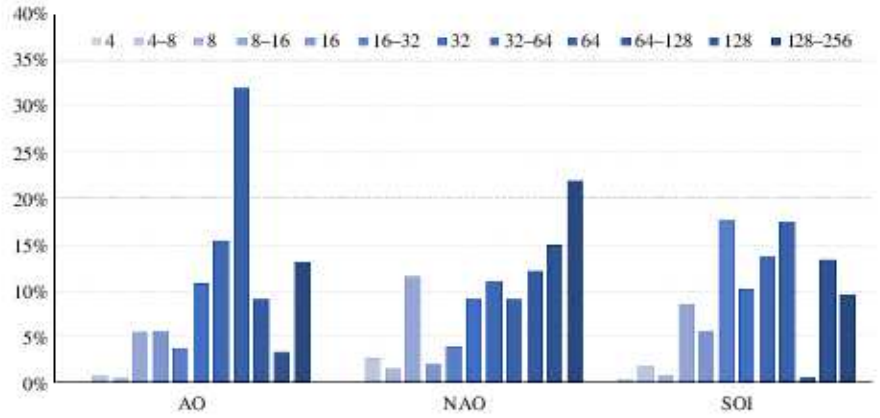

Figure 15. The average distribution of predominant effective periods of the AO, NAO and SOI on the precipitation in Iran.

Iran (see Figure 13 and Table 4). Furthermore, the SOI and ENSO exhibit 2- to 7-year periodicities (Ropelewski and Halpert, 1986), and periods equal to or greater than 2 years were dominant for precipitation and SOI at most of the stations (see Figure 14 and Table 5). It seemed that only the obtained results from the WCO for the AO and precipitation did not have high conformance with the major cycle of the AO, which is estimated to be between 10 and 40 years (Ambaum *et al.*, 2001; ESSEA, 2009). As can be seen in Figure 12 and Table 3, the most dominant period for the NAO and precipitation at most of the stations was around 64 months, which is not similar to the main cycles of the AO. It seems that better and more precise results for the AO could be obtained in this study if the length of precipitation time series were longer. Comparing Figures 10–12 with Figures 1–3, it can be seen that there is no noticeable similarity between the topography pattern (i.e. the shape and spatial distribution of topography or variations in elevation) in Iran and the results for the predominant periodic relationship between precipitation and the three climatic indices. It seems that although the major mountains (i.e. Alborz and Zagros) have noticeable effects on precipitation in Iran, for the assessment of large-scaled climatic indices on precipitation, the topography does not affect the results. The results of this study showed that the WCO is a very good and robust method for detecting the relationship between multiple time series in a time–frequency space. However, in order to obtain more detailed results about the interactions between teleconnections and meteorological

events, more hydro-climatological studies using the WCO are necessary.

6. Conclusions

In this paper, the relationship between three major climatic teleconnections, the AO, NAO and SOI, and precipitation was studied at 30 synoptic stations in Iran from 1960 to 2014, in a time–frequency space, using WCO. The results of this study showed that the SOI is the most effective large scale climatic index for precipitation in Iran, as it has the maximum regions with a 5% significance level in the WCO plots. For the AO index, 64 months was the most predominant and effective period on the precipitation in Iran, while for the NAO, a 128- to 256-month period was the most predominant. The results of this research revealed that studying the relationship between multiple meteorological or hydrological time series in a time–frequency space can be more beneficial compared to traditional correlation methods, and the WCO method is one of the best choices to achieve the correlations in a time–frequency space. The number of hydro-climatological studies in which WCO are used is somewhat scarce, and there is a need for more studies employing this method to obtain more detailed facts about the interactions between large scale and local hydrological and meteorological events.

Acknowledgements

To perform the WPS and WCO methods in this paper, the MATLAB codes provided by A. Grinsted (http://noc.ac.uk/using-science/crosswavelet-wavelet-coherence), and C. Torrence and G. P. Compo (http://paos.colorado.edu/research/wavelets/software.html), were employed, with few modifications.

References

Adamowski J, Chan HF. 2011. A wavelet neural network conjunction model for groundwater level forecasting. *J. Hydrol.* **407**(1–4): 28–40.
Adamowski J, Prokoph A. 2013. Assessing the impacts of the urban heat island effect on streamflow patterns in Ottawa, Canada. *J. Hydrol.* **496**: 225–237.
Adamowski J, Sun K. 2010. Development of a coupled wavelet transform and neural network method for flow forecasting of non-perennial rivers in semi-arid watersheds. *J. Hydrol.* **390**(1–2): 85–91.
Adamowski K, Prokoph A, Adamowski J. 2009. Development of a new method of wavelet aided trend detection and estimation. *Hydrol. Process.* **23**(18): 2686–2696.
Adamowski J, Adamowski K, Prokoph A. 2013. A spectral analysis based methodology to detect climatological influences on daily urban water demand. *Math. Geosci.* **45**(1): 49–68.
Aguado E, Burt JE. 2013. *Understanding Weather and Climate*. Pearson: New York, NY, 576 pp.
Ahrens CD. 2016. *Meteorology Today*. Cengage Learning: Toronto, Canada, 662 pp.
Ambaum MHP, Hoskins BJ, Stephenson DB. 2001. Arctic oscillation or North Atlantic oscillation? *J. Clim.* **14**(16): 3495–3507.
Anctil F, Coulibaly P. 2004. Wavelet analysis of the interannual variability in southern Québec streamflow. *J. Clim.* **17**(1): 163–173.
Araghi A, Mousavi Baygi M, Adamowski J, Malard J, Nalley D, Hasheminia SM. 2015. Using wavelet transforms to estimate surface temperature trends and dominant periodicities in Iran based on gridded reanalysis data. *Atmos. Res.* **155**: 52–72.
Araghi A, Mousavi-Baygi M, Adamowski J. 2016. Detection of trends in days with extreme temperatures in Iran from 1961 to 2010. *Theor. Appl. Climatol.* **125**: 213–225.
Barry RG, Chorley RJ. 2009. *Atmosphere, Weather and Climate*. Routledge: New York, NY, 536 pp.
Bhalme HN, Jadhav SK. 1984. The Southern Oscillation and its relation to the monsoon rainfall. *J. Climatol.* **4**(5): 509–520.
Bosart LF, Bluestein HB. 2008. *Synoptic-Dynamic Meteorology and Weather Analysis and Forecasting*. American Meteorological Society: Boston, MA, 426 pp.
Box GEP, Jenkins GM, Reinsel GC. 2008. *Time Series Analysis, Forecasting and Control*. John Wiley & Sons: Hoboken, NJ, 746 pp.
Brittain JS, Halliday DM, Conway BA, Jens Bo N. 2007. Single-trial multiwavelet coherence in application to neurophysiological time series. *IEEE Trans. Biomed. Eng.* **54**(5): 854–862.
Çağatay Karabörk M, Kahya E. 2003. The teleconnections between the extreme phases of the southern oscillation and precipitation patterns over Turkey. *Int. J. Climatol.* **23**(13): 1607–1625.
Çağatay Karabörk M, Kahya E. 2009. The links between the categorised Southern Oscillation indicators and climate and hydrologic variables in Turkey. *Hydrol. Process.* **23**(13): 1927–1936.
Cayan DR, Dettinger MD, Diaz HF, Graham NE. 1998. Decadal variability of precipitation over western North America. *J. Clim.* **11**(12): 3148–3166.
Cazelles B, Chavez M, Berteaux D, Ménard F, Vik J, Jenouvrier S, Stenseth NC. 2008. Wavelet analysis of ecological time series. *Oecologia* **156**(2): 287–304.
Chang N, Imen S, Mullen L, Chen C, Valdez M, Yang J. 2014. Multisensor analysis of teleconnection signals in relation to terrestrial precipitation and forest greenness in North and Central America. In *Proceedings of the 11th IEEE International Conference on Networking, Sensing and Control, ICNSC 2014*, Miami, FL, 649–654.
Cook ER, D'Arrigo RD, Briffa KR. 1998. A reconstruction of the North Atlantic Oscillation using tree-ring chronologies from North America and Europe. *The Holocene* **8**(1): 9–17.
Coulibaly P. 2006. Spatial and temporal variability of Canadian seasonal precipitation (1900–2000). *Adv. Water Resour.* **29**(12): 1846–1865.
Curry JA, Webster PJ. 1999. *Thermodynamics of Atmospheres and Oceans*. Academic Press: New York, NY, 471 pp.
Di Y, Ding W, Imen S, Chang N-B. 2015. Teleconnection signals effect on terrestrial precipitation: big data analytics vs. wavelet analysis. In *Proceedings of the 5th International Workshop on Climate Informatics*, Boulder, CO.
Dinpashoh Y, Jhajharia D, Fakheri-Fard A, Singh VP, Kahya E. 2011. Trends in reference crop evapotranspiration over Iran. *J. Hydrol.* **399**(3–4): 422–433.
Duhan D, Pandey A. 2013. Statistical analysis of long term spatial and temporal trends of precipitation during 1901–2002 at Madhya Pradesh, India. *Atmos. Res.* **122**: 136–149.
ESSEA. 2009. *Arctic Oscillation*. Earth System Science Education Alliance: Arlington, VA.
Fugal DL. 2009. *Conceptual Wavelets in Digital Signal Processing: An In-depth, Practical Approach for the Non-mathematician*. Space & Signals Technical Publications, 302 pp.
Gan TY, Gobena AK, Wang Q. 2007. Precipitation of southwestern Canada: wavelet, scaling, multifractal analysis, and teleconnection to climate anomalies. *J. Geophys. Res. Atmos.* **112**(D10): D10110, doi: 10.1029/2006JD007157.
Greatbatch RJ. 2000. The North Atlantic oscillation. *Stoch. Env. Res. Risk A.* **14**(4–5): 213–242.
Grinsted A, Moore JC, Jevrejeva S. 2004. Application of the cross wavelet transform and wavelet coherence to geophysical time series. *Nonlinear Processes Geophys.* **11**(5/6): 561–566.
Grossmann A, Morlet J. 1984. Decomposition of Hardy functions into square integrable wavelets of constant shape. *SIAM J. Math. Anal.* **15**(4): 723–736.
Hernández E, Weiss G. 1996. *A First Course on Wavelets. Studies in Advanced Mathematics*. CRC Press: Boca Raton, FL, 489 pp.
Higgins RW, Leetmaa A, Xue Y, Barnston A. 2000. Dominant factors influencing the seasonal predictability of U.S. precipitation and surface air temperature. *J. Clim.* **13**: 3994–4017.
Hurrell J, Van Loon H. 1997. Decadal variations in climate associated with the North Atlantic Oscillation. *Clim. Change* **36**(3–4): 301–326.
Ionita M, Chelcea S, Rimbu N, Adler MJ. 2014. Spatial and temporal variability of winter streamflow over Romania and its relationship to large-scale atmospheric circulation. *J. Hydrol.* **519**(PB): 1339–1349.
Jevrejeva S, Moore JC, Woodworth PL, Grinsted A. 2005. Influence of large-scale atmospheric circulation on European sea level: results

based on the wavelet transform method. *Tellus Ser. A Dyn. Meteorol. Oceanogr.* **57**(2): 183–193.
Jiang R, Gan TY, Xie J, Wang N. 2014. Spatiotemporal variability of Alberta's seasonal precipitation, their teleconnection with large-scale climate anomalies and sea surface temperature. *Int. J. Climatol.* **34**(9): 2899–2917.
Jones PD, Jonsson T, Wheeler D. 1997. Extension to the North Atlantic oscillation using early instrumental pressure observations from Gibraltar and south-west Iceland. *Int. J. Climatol.* **17**(13): 1433–1450.
Karamouz M, Nazif S, Falahi M. 2013. *Hydrology and Hydroclimatology, Principles and Applications*. CRC Press: Boca Raton, FL, 731 pp.
Kreyszig E. 2011. *Advanced Engineering Mathematics*. John Wiley & Sons, Inc.: Hoboken, NJ, 1283 pp.
Küçük M, Kahya E, Cengiz TM, Karaca M. 2009. North Atlantic oscillation influences on Turkish lake levels. *Hydrol. Process.* **23**(6): 893–906.
Kuo C, Gan TY, Yu P. 2010. Wavelet analysis on the variability, teleconnectivity, and predictability of the seasonal rainfall of Taiwan. *Mon. Weather Rev.* **138**(1): 162–175.
Labat D. 2005. Recent advances in wavelet analyses: part 1. A review of concepts. *J. Hydrol.* **314**(1–4): 275–288.
Labat D, Ronchail J, Guyot JL. 2005. Recent advances in wavelet analyses: part 2 - Amazon, Parana, Orinoco and Congo discharges time scale variability. *J. Hydrol.* **314**(1–4): 289–311.
Lau KM, Weng H. 1995. Climate signal detection using wavelet transform: how to make a time series sing. *Bull. Am. Meteorol. Soc.* **76**(12): 2391–2402.
Li X, Gao S. 2012. *Precipitation Modeling and Quantitative Analysis*. Springer: Dordrecht, The Netherlands, 240 pp.
Liu PC. 1994. Wavelet spectrum analysis and ocean wind waves. In *Wavelets in Geophysics*, Foufoula-Georgiou E, Kumar P (eds). Academic Press: New York, NY, 151–166.
Liu LT, Hsu HT, Gnafarend EW. 2005. Wavelet coherence analysis of length-of-day variations and El Niño-Southern Oscillation. *J. Geodyn.* **39**(3): 267–275.
Loucks DP, van Beek E. 2005. *Water Resources Systems Planning and Management*. UNESCO: Paris, France, 680 pp.
Lutgens FK, Tarbuck EJ. 2013. *The Atmosphere, An Introduction to Meteorology*. Prentice Hall: Upper Saddle River, NJ, 528 pp.
Maidment DR. 1993. *Handbook of Hydrology*. McGraw Hill Inc.: New York, NY, 1424 pp.
Mak M. 2011. *Atmospheric Dynamics*. Cambridge University Press: New York, NY, 500 pp.
Mallat S. 2008. *A Wavelet Tour of Signal Processing*. Academic Press: New York, NY, 700 pp.
Maraun D, Kurths J. 2004. Cross wavelet analysis: significance testing and pitfalls. *Nonlinear Processes Geophys.* **11**(4): 505–514.
Martinez CJ, Baigorria GA, Jones JW. 2009. Use of climate indices to predict corn yields in southeast USA. *Int. J. Climatol.* **29**(11): 1680–1691.
Massei N, Durand A, Deloffre J, Dupont J, Valdes D, Laignel B. 2007. Investigating possible links between the North Atlantic Oscillation and rainfall variability in Northwestern France over the past 35 years. *J. Geophys. Res. Atmos.* **112**(D9): D09121, doi: 10.1029/2005JD007000.
Massei N, Laignel B, Deloffre J, Mesquita J, Motelay A, Lafite R, Durand A. 2010. Long-term hydrological changes of the Seine River flow (France) and their relation to the North Atlantic Oscillation over the period 1950–2008. *Int. J. Climatol.* **30**(14): 2146–2154.
Mavi HS, Tupper GJ. 2004. *Agrometeorology, Principles and Applications of Climate Studies in Agriculture*. Food Products Press: Binghamton, NY, 364 pp.
McCuen RH. 1998. *Hydrologic Analysis and Design*. Pearson Education: Hoboken, NJ, 814 pp.
Montgomery DC, Runger GC. 2011. *Applied Statistics and Probability for Engineers*. John Wiley & Sons: Hoboken, NJ, 792 pp.
Mooley DA, Parthasarathy B, Sontakke NA. 1985. Relationship between all-India summer monsoon rainfall and southern oscillation/eastern equatorial Pacific sea surface temperature. *Proc. Indian Acad. Sci. (Earth Planet. Sci.)* **94**(3): 199–210.
Mwale D, Gan T, Devito K, Mendoza C, Silins U, Petrone R. 2009. Precipitation variability and its relationship to hydrologic variability in Alberta. *Hydrol. Process.* **23**(21): 3040–3056.
Nalley D, Adamowski J, Khalil B, Ozga-Zielinski B. 2013. Trend detection in surface air temperature in Ontario and Quebec, Canada during 1967–2006 using the discrete wavelet transform. *Atmos. Res.* **132–133**: 375–398.
Nievergelt Y. 2001. *Wavelets Made Easy*. Birkhäuser, 297 pp.
Niu J, Chen J, Sivakumar B. 2014. Teleconnection analysis of runoff and soil moisture over the Pearl River basin in southern China. *Hydrol. Earth Syst. Sci.* **18**(4): 1475–1492.
Nourani V, Hosseini Baghanam A, Adamowski J, Kisi O. 2014. Applications of hybrid wavelet–Artificial Intelligence models in hydrology: a review. *J. Hydrol.* **514**: 358–377.
Olkkonen H. 2011. *Discrete Wavelet Transform – Biomedical Application*. InTech: Rijeka, Croatia, 366 pp.
Oppenheim AV, Schafer RW, Buck JR. 1999. *Discrete-Time Signal Processing*. Prentice-Hall, Inc.: Upper Saddle River, NJ, 870 pp.
Ouachani R, Bargaoui Z, Ouarda T. 2013. Power of teleconnection patterns on precipitation and streamflow variability of upper Medjerda Basin. *Int. J. Climatol.* **33**(1): 58–76.
Partal T, Küçük M. 2006. Long-term trend analysis using discrete wavelet components of annual precipitations measurements in Marmara region (Turkey). *Phys. Chem. Earth* **31**(18): 1189–1200.
Percival DB, Walden AT. 2000. *Wavelet Methods for Time Series Analysis*. Cambridge University Press: New York, NY, 594 pp.
Rakhecha PR, Singh VP. 2009. *Applied Hydrometeorology*. Springer: Dordrecht, The Netherlands, 384 pp.
Risko SL, Martinez CJ. 2014. Forecasts of seasonal streamflow in West-Central Florida using multiple climate predictors. *J. Hydrol.* **519**(Part A): 1130–1140.
Rogers JC. 1984. The association between the North Atlantic oscillation and the Southern oscillation in the Northern Hemisphere. *Mon. Weather Rev.* **112**(10): 1999–2015.
Ropelewski CF, Halpert MS. 1986. North American precipitation and temperature patterns associated with the El Niño/Southern oscillation (ENSO). *Mon. Weather Rev.* **114**(12): 2352–2362.
Rossi A, Massei N, Laignel B. 2011. A synthesis of the time-scale variability of commonly used climate indices using continuous wavelet transform. *Glob. Planet. Chang.* **78**(1–2): 1–13.
Saha K. 2008. *The Earth's Atmosphere, Its Physics and Dynamics*. Springer: Berlin, Germany, 370 pp.
Sang Y-F. 2013. A review on the applications of wavelet transform in hydrology time series analysis. *Atmos. Res.* **122**: 8–15.
Shabbar A, Bonsal B, Khandekar M. 1997. Canadian precipitation patterns associated with the Southern oscillation. *J. Clim.* **10**(12): 3016–3027.
Shelton M. 2009. *Hydroclimatology, Perspectives and Applications*. Cambrigde University Press: New York, NY, 438 pp.
Shrestha LM. 2000. Interannual variation of summer monsoon rainfall over Nepal and its relation to Southern Oscillation Index. *Meteorol. Atmos. Phys.* **75**(1): 21–28.
Thompson DWJ, Wallace JM. 1998. The Arctic oscillation signature in the wintertime geopotential height and temperature fields. *Geophys. Res. Lett.* **25**(9): 1297–1300.
Torrence C, Compo GP. 1998. A practical guide to wavelet analysis. *Bull. Am. Meteorol. Soc.* **79**(1): 61–78.
Torrence C, Webster PJ. 1999. Interdecadal changes in the ENSO–monsoon system. *J. Clim.* **12**(8): 2679–2690.
Unal YS, Deniz A, Toros H, Incecik S. 2012. Temporal and spatial patterns of precipitation variability for annual, wet, and dry seasons in Turkey. *Int. J. Climatol.* **32**(3): 392–405.
Velasco VM, Mendoza B. 2008. Assessing the relationship between solar activity and some large scale climatic phenomena. *Adv. Space Res.* **42**(5): 866–878.
Von Storch H, Zwiers FW. 1999. *Statistical Analysis in Climate Research*. Cambridge University Press: New York, NY, 484 pp.
Wallace JM, Gutzler DS. 1981. Teleconnections in the geopotential height field during the Northern Hemisphere winter. *Mon. Weather Rev.* **109**(4): 784–812.
Wang H, Chen Y, Pan Y, Li W. 2015. Spatial and temporal variability of drought in the arid region of China and its relationships to teleconnection indices. *J. Hydrol.* **523**: 283–296.
Wilhite DA. 2005. *Drought and Water Crises: Science, Technology, and Management Issues*. Taylor and Francis: Abingdon, UK, 406 pp.
Wilks DS. 2011. *Statistical Methods in the Atmospheric Science*. International Geophysics. Academic Press: New York, NY, 704 pp.
Yan Z, Tsimplis MN, Woolf D. 2004. Analysis of the relationship between the North Atlantic oscillation and sea-level changes in northwest Europe. *Int. J. Climatol.* **24**(6): 743–758.
Yarnal B, Diaz HF. 1986. Relationships between extremes of the Southern oscillation and the winter climate of the Anglo-American Pacific Coast. *J. Climatol.* **6**(2): 197–219.

